Numerical simulation of a guitar

Eliane Bécache, Antoine Chaigne, Grégoire Derveaux, Patrick Joly

NUMERICAL SIMULATION OF A GUITAR

ELIANE BÉCACHE*, ANTOINE CHAIGNE†, GRÉGOIRE DERVEAUX*‡, AND PATRICK JOLY*

Abstract.
The purpose of this study is to present a time-domain numerical modeling of the guitar. The model involves the transverse displacement of the string excited by a force pulse, the flexural motion of the soundboard and the sound radiation in the air. We use a specific spectral method for solving the Kirchhoff-Love's dynamic plate model for orthotropic material, a fictitious domain method for solving the fluid-structure interaction and a conservative scheme for the time discretization. One of the originality of the proposed scheme is a stable coupling method between a continuous time resolution and a discrete one.

Key words. Kirchhoff-Love's plate model, fluid-structure interaction, mixed finite elements, fictitious domain method, spectral method, energy method, stability.

AMS subject classifications. 65M12, 65M60, 65M70.

1. Introduction. The purpose of the presented study is the numerical resolution of a physical modeling of the acoustic guitar. This work is part of the general framework *time domain modeling of musical instruments* initiated about 10 years ago by A. Chaigne, which purpose is to better understand the vibroacoustical behavior of instruments by use of an accurate physical modeling and advanced numerical methods. The interest of the time-domain approach instead of the more usual frequency-domain approach, is the accuracy in the modeling of the coupling between the different parts of the instrument. Such a model constitutes a virtual instrument in which it is possible to change easily the geometrical or physical parameters. It will thus be of great help to develop tools for instrument making, sound recording or psychoacoustic studies. Among other works realized in this general framework, we can mention the modeling of the damping in the guitar top plate made by Chaigne and Lambourg [10] and the numerical modeling of the timpani [37].

The instrument is considered as a set of simple structures which are coupled to each other. Since we wish to focus on the modeling of the soundboard and on the fluid-structure interaction, the model used for the other parts of the instrument is intentionally kept simple. An idealized plucking force is acting on a 1D damped string model. The string is coupled to the soundboard via the bridge. The soundboard is modeled as an orthotropic heterogeneous damped Kirchhoff-Love plate, with a soundhole, clamped at its boundaries. The other parts of the body (back, neck, sides...) are assumed to be perfectly rigid. The plate radiates both inside the cavity and in the external free field. The modeling of the complete 3D sound field is a new approach comparing to almost all previous works on the guitar, where the cavity is taken into account as a simple oscillator.

The well posedness of the model is shown with the help of the Hille-Yosida theorem. One of the main difficulty raised by its numerical resolution is that the domain of computation for the sound radiation is a 3D unbounded domain, which involve the complex geometry of the guitar. In addition, a guitar sound can last up to 6 seconds, so that the number of iterations may be great (typically 300,000 time steps for 6s

* INRIA Roquencourt, Projet Ondes, 78153 Le Chesnay Cedex, FRANCE.
† ENSTA-UME, Chemin de la Hunière, 91761 Palaiseau Cedex. FRANCE
‡Mathematic Department, Stanford University. Email: derveaux@stanford.edu

of sound). It is thus of great importance to define an efficient resolution scheme. In order to circumvent these difficulties, the fluid-structure interaction problem is solved with the help of a fictitious domain method which main interest is to allow the use of a regular mesh for the approximation of the acoustic field while the geometry of the instrument is taken into account with an accurate triangular surface mesh. For the time discretization, conservative centered finite differences are used. To simulate the free space, the computations are restricted to a box of finite size with the help of higher oder absorbing boundary conditions.

Another important difficulty to cope with this model is the resolution of the Kirchhoff-Love's dynamic plate equation which includes a fourth order space operator and is intrinsically dispersive, which complicates both space and time discretization. We have chosen to solve it with a spectral method, which is particularly efficient in the case of a great number of iterations: the eigenmodes are calculated with a non standard higher order mixed finite elements method, based on a velocity-moment formulation and the spatial semi-discretized problem is solved analytically in time.

The string equation is solved using standard mixed finite elements of lower order on a regular mesh and explicit centered finite differences are used.

The stability of the coupled scheme is ensured through a discrete energy identity. In this aim, the spatial discretization of the equations of the model is based on a mixed variational formulation of the complete system. The time stepping is chosen in such a way that almost all computations, and in particular the 3D computations, are explicit. The resolution of the scheme involves only the inversion at each time step of a small sparse symmetric positive matrix which arises from the fictitious domain resolution of the fluid-structure interaction.

The main originality of the proposed scheme is certainly that it is a stable coupling method between a continuous time resolution (for the plate) and a discrete one (for the string and the air). In addition, the two stability conditions of the complete scheme are exactly the same than the usual CFL conditions obtained for the standard finite difference discretization of the uncoupled 1D and 3D wave equation. This result shows the robustness of the coupling scheme.

The paper is organized as follow: section 2 is devoted to the description of the guitar and the presentation of the model. Section 3 presents the main results of the mathematical analysis of this model: well-posedness and energy identity of the continuous problem. Since it is solved with a spectral method whereas all other equations are solved with finite elements in space and finite differences in time, the numerical resolution of the plate equation takes a particular place and is thus presented in section 4. The numerical scheme of the complete problem is then presented in details in section 5. The well-posedness of this scheme and the stability analysis are discussed in section 6 and finally in section 7, numerical results are given.

2. The model.

2.1. Description of the guitar. The body of guitar is made up of the soundboard, the sides, the back and the neck. The 6 string are attached on one side to the neck and on the other side to the bridge. The soundboard itself is a thin wooden layer containing a sound hole and reinforced by struts (pieces of hard wood glued on its internal face which have a great influence on the shape of the structural modes of the soundboard and on the radiation efficiency of the guitar [39, 35]). The sound produced by a string is appreciated since antiquity for its natural harmonic properties. Unfortunately, this sound is practically inaudible because of its very small diameter. The vibrations of the string are thus transmitted to the soundboard, which large area

ensures efficient coupling to the air. In addition, the soundboard is itself coupled to an acoustic cavity pierced by a hole in order to reinforce the sound power in the low frequency range, by the help of the Helmholtz resonance frequency [40, 23].

The following assumptions were made in order to propose a physical modeling of the instrument:

- the amplitudes of vibration are small, which justify a linear model,
- the body has no thickness and the neck is neglected,
- only the soundboard vibrate (the rest of the body is supposed perfectly rigid),
- the soundboard is modeled using a Kirchhoff-Love flexural plate equation (the motion parallel to the medium plan is neglected). The struts and the bridge are considered as heterogeneities,
- only the transverse polarization of the string is considered: the in-plane displacement of the string (parallel to the soundboard) is neglected,
- the string is excited with an idealized plucking force,
- the internal phenomena of damping in the plate and in the string are modeled by dissipative terms of viscoelastic type.

Geometrical description. The body of the guitar is delimited by a surface denoted Γ which is divided into two parts: $\Gamma = \omega \cup \Sigma$, where ω is the top plate of the instrument and Σ is the rest of the surface (*ie.* sides and back). The boundary of ω itself is divided into two parts: γ_0 is the outer boundary of the top plate and γ_f is the inner boundary, along the hole. The surrounding air occupies the domain $\Omega = \mathbb{R}^3 \setminus \Gamma$. The string of length l_s is rigidly fixed to the neck at a point denoted O, chosen as origin of the coordinate system (see Fig. 2.1).

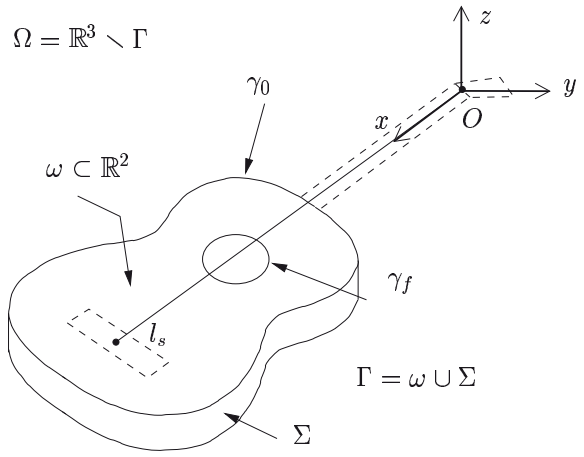

FIG. 2.1. *Geometrical description of the guitar*

Unknowns. This model includes the following unknowns, all time dependent:

• the vertical displacement of the string	$u_s(x,t)$,	$x \in]0, l_s[$;
• the vertical displacement of the soundboard	$u_p(x,y,t)$,	$(x,y) \in \omega$:
• the acoustic pressure	$p(x,y,z,t)$,	$(x,y,z) \in \Omega$;
• the acoustic velocity field	$\underline{\mathbf{v}}_a(x,y,z,t)$,	$(x,y,z) \in \Omega$.

Notations. A simple underlined quantity (*e.g.* $\underline{\theta}$) denotes a vector in $\mathbb{R}^2$, a double underlined quantity (*e.g.* $\underline{\underline{\mathcal{M}}}$) denotes a tensor of second order in $\mathbb{R}^2$ and a bold simple underlined quantity (*e.g.* $\underline{\mathbf{N}}$) denotes a vector in $\mathbb{R}^3$. div denotes the usual divergence operator for vectors and $\underline{\nabla}$ denotes the usual gradient operator for

scalars. $\underline{\mathrm{Div}}$ denotes the divergence operator for tensors defined by:

$$\underline{\mathrm{Div}}\,\underline{\underline{\mathcal{M}}} = \begin{pmatrix} \partial_1\mathcal{M}_{11} + \partial_2\mathcal{M}_{12} \\ \partial_1\mathcal{M}_{21} + \partial_2\mathcal{M}_{22} \end{pmatrix}$$

$\underline{\underline{\varepsilon}}(\underline{\theta})$ denotes the plane linearized strain tensor of the vector field $\underline{\theta}$, defined by:

$$\varepsilon_{\alpha\beta}(\underline{\theta}) = \frac{1}{2}(\partial_\beta\theta_\alpha + \partial_\alpha\theta_\beta), \quad \forall\alpha,\beta \in \{1,2\}.$$

2.2. Equations. This model of guitar is described by the following set of equations:

Equations for the string:

$$(2.1)\qquad \begin{cases} (a) \quad \rho_s\dfrac{\partial^2 u_s}{\partial t^2} - T(1+\eta_s\dfrac{\partial}{\partial t})\dfrac{\partial^2 u_s}{\partial x^2} = f_s(x,t), & \text{in }]0,l_s[, \\ (b) \quad u_s(0,t) = 0, & \forall t>0, \\ (c) \quad u_s(l_s,t) = \displaystyle\int_\omega G(x,y)u_p(x,y,t)dxdy, & \forall t>0. \end{cases}$$

Equations for the soundboard :

$$(2.2)\qquad \begin{cases} (a) \quad a\rho_p\dfrac{\partial^2 u_p}{\partial t^2} + \mathrm{div}\,\underline{\mathrm{Div}}\,\underline{\underline{\mathcal{M}}} = -[p]_\omega + \mathcal{F}(x,y,t) & \text{in } \omega, \\ (b) \quad \underline{\underline{\mathcal{M}}} = a^3\mathbf{C}\,(1+\eta_p\dfrac{\partial}{\partial t})\underline{\underline{\varepsilon}}\,(\underline{\nabla}u_p) & \text{in } \omega, \\ (c) \quad \mathcal{F}(x,y,t) = G(x,y)T(1+\eta_s\dfrac{\partial}{\partial t})\dfrac{\partial u_s}{\partial x}(l_s,t) & \text{in } \omega, \\ (d) \quad u_p = 0 \ \text{ and } \ \partial_n u_p = 0, & \text{on } \gamma_0, \\ (e) \quad (\underline{\underline{\mathcal{M}}}\,\underline{n}).\underline{n} = 0 \ \text{ and } \ (\underline{\mathrm{Div}}\,\underline{\underline{\mathcal{M}}}).\underline{n} + \partial_\tau[(\underline{\underline{\mathcal{M}}}\,\underline{n}).\underline{\tau}] = 0, & \text{on } \gamma_f. \end{cases}$$

Equations for the surrounding air:

$$(2.3)\qquad \begin{cases} (a) \quad \rho_a\dfrac{\partial \underline{\mathbf{v}}_a}{\partial t} + \underline{\nabla}p = 0, & \text{in } \Omega, \\ (b) \quad \mu_a\dfrac{\partial p}{\partial t} + \mathrm{div}\,\underline{\mathbf{v}}_a = 0, & \text{in } \Omega, \\ (c) \quad \underline{\mathbf{v}}_a(x,y,0,t).\underline{e}_z = u_p(x,y,t), & \forall (x,y)\in\omega, \\ (d) \quad \underline{\mathbf{v}}_a(x,y,z,t).\underline{\mathbf{N}} = 0, & \forall (x,y,z)\in\Sigma. \end{cases}$$

At the origin, the whole system is at rest. These initial conditions will be systematically omitted in the following. The previous set of equations ((2.1), (2.2), (2.3)) is denoted $\mathcal{P}_g$ and is described below.

- (2.1a) is the 1D wave equation describing the displacement of the string. T is the uniform tension, ρ_s is the uniform lineic density. η_s is an internal dissipative term of viscoelastic type. On the right hand side, the force f_s exerted by the finger is assumed to be an imposed force $f_s(x,t) = g(x)h(t)$, where the

C^1 function $h(t)$ represents a simple idealized version of the "stick-slip" mechanism that governs the interaction between string and finger (Fig. 2.2a). This force is distributed over a small segment of the string by means of the smooth positive function g, normalized so that $\int_0^{l_s} g(x)dx = 1$ (Fig. 2.2b). Despite its simplicity, this excitation is in fairly good agreement with experiments [9].

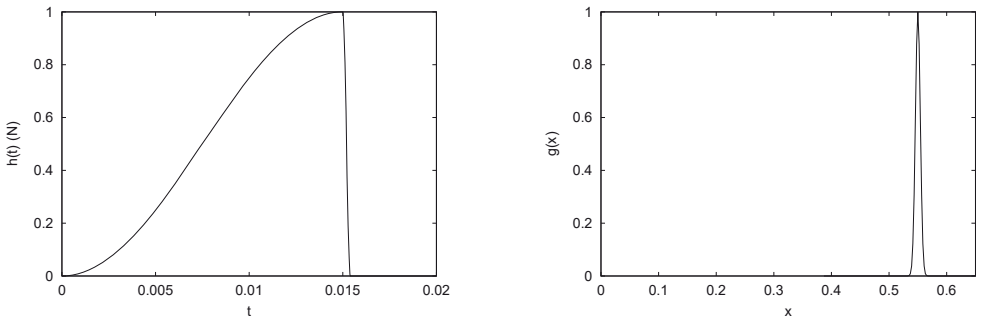

(a) (b)

FIG. 2.2. *Idealized plucking force. (a) Time dependence. (b) Space dependence*

- (2.1b) expresses that the string is fixed at the neck and (2.1c) expresses that the string and the soundboard are always in contact at the bridge. The motion of the string at the bridge is thus given by the mean displacement of a small plate's area. G is positive and normalized so that $\int_\omega G = 1$
- (2.2a) is the Kirchhoff-Love equation describing the flexural displacement of the soundboard [20, 13, 33]. $a = a(x, y)$ is the thickness and $\rho_p = \rho_p(x, y)$ the density. On the right hand side, the force exerted by the surrounding air is $[p]_\omega = p_e - p_i$, the pressure jump across the soundboard, where p_e and p_i denotes the external and internal pressure respectively and $\mathcal{F}$ is force exerted by the string (see below).
- (2.2b) is the analogous of Hooke's law for a Kirchhoff-Love's plate. $\underline{\underline{\mathcal{M}}}$ denotes the bending moment. It is a symmetric tensor of second order. η_p is a uniform dissipative term of viscoelastic type. $\mathbf{C} = \mathbf{C}(x, y)$ is the rigidity tensor for orthotropic materials. $\mathbf{C}$ can be written:

$$\mathbf{C} = c_{11} \begin{pmatrix} 1 & \tilde{c}_{12} & 0 \\ \tilde{c}_{12} & \tilde{c}_{22} & 0 \\ 0 & 0 & \tilde{c}_{33} \end{pmatrix} = c_{11}\tilde{\mathbf{C}}, \tag{2.4}$$

  where c_{11} is an elastic coefficient in Pa and $\tilde{c}_{12}, \tilde{c}_{22}$ and $\tilde{c}_{33}$, are dimensionless coefficient. $\mathbf{C}$ is supposed to satisfy: $0 < c^- \left|\underline{\underline{\mathcal{M}}}\right|^2 \leq \mathbf{C}\,\underline{\underline{\mathcal{M}}} : \underline{\underline{\mathcal{M}}} \leq c^+ \left|\underline{\underline{\mathcal{M}}}\right|^2$
- The force $\mathcal{F}$ exerted by the string on the plate is assumed to be the normal component of the tension of the string at this point (this is a common assumption [23]). This force is distributed over the small plate's area defined by the spatial window G used above. For a non dissipative string, considering small displacements, it is given by:

$$\mathcal{F}(x, y, t) \approx -T\partial_x u_s(l_s, t)G(x, y), \tag{2.5}$$

  One should modify this last equation in order to take into account the viscoelastic dissipation in the string, which leads to (2.2c).

- The conditions (2.2d) express that the plate is clamped along its outer boundary γ_0, while the conditions (2.2e) express that the plate is free along the soundhole γ_f. $\underline{n}$ denotes the outer normal and $\underline{\tau}$ denotes the tangential vector along the boundary $\delta\omega$. ∂_n and ∂_s denote the normal and tangential derivative operator along the boundary $\delta\omega$ respectively.
- (2.3a) and (2.3b) are the linearized Euler's equations for the acoustic field. ρ_a is the density of the air and $\mu_a = \frac{1}{\rho_a c_a^2}$ is the permitivity of the air where c_a is the speed of sound in the air.
- (2.3c) expresses the continuity of the normal component of the acoustic velocity on ω, which is the standard fluid-structure interaction condition and (2.3d) expresses that the rest of the body is perfectly rigid. $\underline{\mathbf{N}}$ denotes the outer normal to the boundary Σ.

3. Mathematical analysis. It is not difficult to show that the problem $\mathcal{P}_g$ is well posed. In fact, the proof of the Hille-Yosida theorem's hypothesis [42] is long but straightforward. One should only take care to the treatment of the free boundary conditions of the soundboard which must be seen in a weak way [17]. One has:

THEOREM 3.1 (Well posedness of the problem $\mathcal{P}_g$). *The plucking of the string is supposed to satisfy:*

$$f_s \in C^1(\mathbb{R}_+, L^2(]0, l_s[)),$$

then problem $\mathcal{P}_g$ admits a unique strong solution $(u_s, u_p, p, \underline{\mathbf{v}}_a)$ such that:

$$\left\{\begin{array}{l} u_s \in C^2(\mathbb{R}+, L^2(]0, l_s[)) \cap C^1(\mathbb{R}_+, \mathcal{V}_s), \\ \left[(1+\eta_s\frac{\partial}{\partial t})\frac{\partial^2 u_s}{\partial x^2}\right] \in C^0(\mathbb{R}_+, L^2(]0, l_s[)), \\ u_p \in C^2(\mathbb{R}+, L^2(\omega)) \cap C^1(\mathbb{R}_+, \mathcal{V}_p), \\ \left[(1+\eta_p\frac{\partial}{\partial t})\,\mathrm{div}\,\underline{\mathrm{Div}}\,\mathbf{C}\,\underline{\underline{\varepsilon}}\,(\underline{\nabla} u_p)\right] \in C^0(\mathbb{R}_+, L^2(\omega)), \\ p \in C^1(\mathbb{R}_+, L^2(\Omega)) \cap C^0(\mathbb{R}_+, H^1(\Omega)), \\ \underline{\mathbf{v}}_a \in C^1(\mathbb{R}_+, (L^2(\Omega))^3) \cap C^0(\mathbb{R}_+, H(\mathrm{div}, \Omega)), \end{array}\right. \tag{3.1}$$

with $\mathcal{V}_s = \{u_s \in H^1(]0, l_s[)\ ;\ u_s(0) = 0\}$ and $\mathcal{V}_p = \{u_p \in H^2\ ; u_p = \partial_n u_p = 0$ on $\gamma_0\}$. The boundary conditions are verified in the following sense:

$$\left|\begin{array}{l} u_s(l_s, t) = \displaystyle\int_\omega G(x,y) u_p(x,y,t)\,dxdy, \quad \text{in } C^1(\mathbb{R}+, \mathbb{R}), \\ \left\{\begin{array}{l} \forall u_p^* \in \mathcal{V}_p, \quad (1+\eta_p\frac{\partial}{\partial t})\displaystyle\int_\omega \mathrm{div}\,\underline{\mathrm{Div}}\,\mathbf{C}\,\underline{\underline{\varepsilon}}\,(\underline{\nabla} u_p)\,u_p^* \\ \qquad = (1+\eta_p\frac{\partial}{\partial t})\displaystyle\int_\omega \mathbf{C}\,\underline{\underline{\varepsilon}}(\underline{\nabla} u_p) : \underline{\underline{\varepsilon}}(\underline{\nabla} u_p^*), \quad \text{in } C^0(\mathbb{R}+, \mathbb{R}), \end{array}\right. \\ \underline{\mathbf{v}}_a \cdot \underline{\mathbf{N}} = \dfrac{\partial \tilde{u}_p}{\partial t}, \quad \text{in } C^0(\mathbb{R}_+, H^{-\frac{1}{2}}(\Gamma)), \end{array}\right. \tag{3.2}$$

where the extension of $\dfrac{\partial u_p}{\partial t}$ to Γ is defined by: $(\dfrac{\partial \tilde{u}_p}{\partial t})_{|\omega} = \dfrac{\partial u_p}{\partial t}$, and $(\dfrac{\partial \tilde{u}_p}{\partial t})_{|\Sigma} = 0$.

This result is based essentially on the following energy identity, which shows that the energy of the complete system decreases with time, when it is free oscillating. It is

of particular interest for obtaining a priori estimates of the solution given in Theorem 3.1. Furthermore a similar identity will be exploited for ensuring the stability of the numerical resolution scheme.

THEOREM 3.2 (Energy identity). *The unique strong solution* $(u_s, u_p, p, \underline{\mathbf{v}}_a)$ *of problem* $\mathcal{P}_g$ *satisfies:*

$$\frac{dE}{dt}(t) = \int_0^{l_s} f_s \frac{\partial u_s}{\partial t} - \int_0^{l_s} \eta_s T \left| \frac{\partial^2 u_s}{\partial x \partial t} \right|^2 - \int_\omega \eta_p a^3 \mathbf{C}\, \underline{\underline{\varepsilon}}(\underline{\nabla} \partial_t u_p) : \underline{\underline{\varepsilon}}(\underline{\nabla} \partial_t u_p) \tag{3.3}$$

where the total energy $E(t)$ *is defined by* $E(t) = E_s(t) + E_p(t) + E_a(t)$ *with:*

$$\left| \begin{array}{l} E_s(t) = \dfrac{1}{2} \displaystyle\int_0^{l_s} \rho_s \left| \frac{\partial u_s}{\partial t} \right|^2 + \frac{1}{2} \int_0^{l_s} T \left| \frac{\partial u_s}{\partial x} \right|^2, \\ \\ E_p(t) = \dfrac{1}{2} \displaystyle\int_\omega \rho_p \left| \frac{\partial u_p}{\partial t} \right|^2 + \frac{1}{2} \int_\omega \mathbf{C}\, \underline{\underline{\varepsilon}}(\underline{\nabla} u_p) : \underline{\underline{\varepsilon}}(\underline{\nabla} u_p), \\ \\ E_a(t) = \dfrac{1}{2} \displaystyle\int_\Omega \mu_a |p|^2 + \frac{1}{2} \int_\Omega \rho_a |\underline{\mathbf{v}}_a|^2. \end{array} \right.$$

Proof.

1. Equation (2.1a) is multiplied by $\dfrac{\partial u_s}{\partial t}$ and integrated on $]0, l_s[$. Using integration by parts for the second term and the boundary conditions (2.1b) and (2.1c) differentiated in time, one obtains:

$$\frac{dE_c}{dt}(t) + \int_0^{l_s} \eta_s T \left| \frac{\partial^2 u_s}{\partial x \partial t} \right|^2 - \left[T(1 + \eta_s \frac{\partial}{\partial t}) \frac{\partial u_s}{\partial x}(l_s, t) \right] \int_\omega G \frac{\partial u_p}{\partial t} = \int_0^{l_s} f_s \frac{\partial u_s}{\partial t} \tag{3.4}$$

2. We recall the double integration by part formula for a C^1 domain ω (see [12]):

$$\left| \begin{array}{l} \forall\, \underline{\underline{\mathcal{M}}} \in (H^2(\omega))^3 \text{ and } \forall\, u_p \in H^2(\omega) \\ \displaystyle\int_\omega (\operatorname{div} \underline{\operatorname{Div}}\, \underline{\underline{\mathcal{M}}})\, u_p = \int_\omega \underline{\underline{\mathcal{M}}} : \underline{\underline{\varepsilon}}(\underline{\nabla} u_p) + \int_{\delta\omega} \left[(\underline{\underline{\mathcal{M}}}\, \underline{n}).\underline{n} \right] \partial_n u_p \\ \qquad\qquad + \displaystyle\int_{\delta\omega} \left[(\underline{\operatorname{Div}}\, \underline{\underline{\mathcal{M}}}).\underline{n} + \partial_\tau [(\underline{\underline{\mathcal{M}}}\, \underline{n}).\underline{\tau}] \right] u_p. \end{array} \right. \tag{3.5}$$

Equation (2.2a) is multiplied by $\dfrac{\partial u_p}{\partial t}$ and integrated on ω. Then using (3.5), the constitutive law (2.2b) and the boundary conditions (2.2d) and (2.2e), one obtains:

$$\frac{dE_p}{dt}(t) + \int_\omega \eta_p a^3 \mathbf{C}\, \underline{\underline{\varepsilon}}(\underline{\nabla} \partial_t u_p) : \underline{\underline{\varepsilon}}(\underline{\nabla} \partial_t u_p) = - \int_\omega [p]_\omega \frac{\partial u_p}{\partial t} - \left[T(1 + \eta_s \frac{\partial}{\partial t}) \frac{\partial u_s}{\partial x}(l_s, t) \right] \int_\omega G \frac{\partial u_p}{\partial t}. \tag{3.6}$$

3. Equation (2.3a) is multiplied by $\underline{\mathbf{v}}_a$ and integrated on Ω. The second term is integrated by part using the boundary conditions (2.3c) and (2.3d). Equation (2.3b) is multiplied by p and integrated on Ω. The sum of the two previous results gives:

$$\frac{dE_a}{dt}(t) - \int_\omega [p]_\omega \frac{\partial u_p}{\partial t} = 0. \tag{3.7}$$

4. Finally the identity (3.3) is obtained by adding (3.4), (3.6) and (3.7). □

4. The plate problem. The numerical method presented in this section is a summary of the results presented in [17]. In this section the forces exerted on the plate by the air and by the string are supposed to be known and are denoted $f_p(x,y,t)$.

4.1. A mixed variational formulation. The natural variational formulation for the undamped plate problem (2.2) is:

$$\left\{\begin{array}{l} \text{Find } u_p : [0,T] \to V \text{ such that :} \\ \dfrac{d^2}{dt^2}\displaystyle\int_\omega a\rho_p u_p u_p^* + \int_\omega a^3 \mathbf{C}\,\varepsilon(\underline{\nabla} u_p) : \varepsilon(\underline{\nabla} u_p^*) = \int_\omega f_p u_p^*, \quad \forall u_p^* \in V, \end{array}\right. \tag{4.1}$$

where $V = \left\{u_p \in H^2(\omega)\ ;\ u_p = \partial_n u_p = 0 \text{ on } \gamma_0\right\}$. Using the Korn inequality and usual properties of the space $H^2(\omega)$, it is easy to show that the variational formulation (4.1) is well posed. A well known difficulty of this approach is that it requires the use of sophisticated finite elements of class C^1 in order to make an internal approximation of the space $H^2(\omega)$, like for example Argyris finite element [1]. Many methods have been proposed to circumvent this problem [29, 5, 19, 8, 11]. In the present study, following an idea proposed by Glowinsky [26] and then by Ciarlet and Raviart [22] for the static homogeneous isotropic clamped plate, the velocity $v_p = \partial_t u_p$ and the bending moment $\underline{\underline{\mathcal{M}}}$ are used. The problem (2.2) is thus written in the following equivalent form of first order in time and second order in space:

$$\left\{\begin{array}{lll} (a) & a\rho_p \partial_t v_p + \operatorname{div} \underline{\operatorname{Div}}\, \underline{\underline{\mathcal{M}}} = f_p, & \text{in } \omega, \\ (b) & \partial_t \underline{\underline{\mathcal{M}}} = a^3 \mathbf{C}\,(1+\partial_t)\underline{\underline{\varepsilon}}\,(\underline{\nabla} v_p), & \text{in } \omega, \\ (c) & v_p = 0 \ \text{ and } \ \partial_n v_p = 0, & \text{on } \gamma_0, \\ (d) & (\underline{\underline{\mathcal{M}}}\,\underline{n}).\underline{n} = 0 \ \text{ and } \ (\underline{\operatorname{Div}}\, \underline{\underline{\mathcal{M}}}).\underline{n} + \partial_\tau[(\underline{\underline{\mathcal{M}}}\,\underline{n}).\underline{\tau}] = 0, & \text{on } \gamma_f. \end{array}\right. \tag{4.2}$$

The variational formulation of (4.2) is obtained by multiplying (4.2a) by a test function v_p^* and (4.2b) by a test function $\underline{\underline{\mathcal{M}}}^*$. Then using integration by parts over ω and the boundary conditions (4.2c) and (4.2d) leads to:

$$\left\{\begin{array}{ll} \text{Find } v_p : [0,T] \to \mathcal{V} \text{ and } \underline{\underline{\mathcal{M}}} : [0,T] \to \mathcal{X} \text{ such that :} & \\ \dfrac{d}{dt}\displaystyle\int_\omega \rho_p v_p v_p^* - h(\underline{\underline{\mathcal{M}}}, v_p^*) = \int_\omega f_p v_p^*, & \forall v_p^* \in \mathcal{V}, \\ \dfrac{d}{dt}\displaystyle\int_\omega a^{-3}\mathbf{C}^{-1}\,\underline{\underline{\mathcal{M}}} : \underline{\underline{\mathcal{M}}}^* + (1+\eta_p \dfrac{d}{dt}) h(\underline{\underline{\mathcal{M}}}, v_p^*) = 0, & \forall \underline{\underline{\mathcal{M}}}^* \in \mathcal{X}, \end{array}\right. \tag{4.3}$$

where:

$$\mathcal{V} = \left\{v_p \in H^1(\omega)\ ;\ v_p = 0 \text{ on } \gamma_0\right\}$$

$$\mathcal{X} = \left\{(H^1(\omega))^3\ ;\ (\underline{\underline{\mathcal{M}}}\,\underline{n})\,.\,\underline{n} = 0 \text{ on } \gamma_f\right\}.$$

and where we have set

$$h(\underline{\underline{\mathcal{M}}}, v_p) = \int_\omega \underline{\operatorname{Div}}\, \underline{\underline{\mathcal{M}}}\,.\underline{\nabla} v_p + \langle \partial_\tau[(\underline{\underline{\mathcal{M}}}\,\underline{n}).\underline{\tau}], v_p\rangle_{\gamma_f}, \quad \forall \underline{\underline{\mathcal{M}}} \in \mathcal{X}, \forall v_p \in \mathcal{V} \tag{4.4}$$

$\langle .,. \rangle_{\gamma_f}$ denotes the duality bracket in $H^{-\frac{1}{2}}(\gamma_f) \times H^{\frac{1}{2}}(\gamma_f)$.

The main interest of this formulation compared to the natural formulation (4.1) is that it can be discretized with standard Lagrange finite elements for the internal approximation of $H^1(\omega)$.

4.2. Space approximation. Finite dimensional subspaces $\mathcal{V}_h \subset \mathcal{V}$ and $\mathcal{X}_h \subset \mathcal{X}$ are introduced. More precisely, let ω_h be a triangular mesh of the soundboard and $\mathcal{P}$ be a set of polynomial functions to be determined. Then one introduces:

$$\mathcal{V}_h = \left\{ v^*_{p_h} \in \mathcal{V} \ , \ v^*_{p_h|K} \in \mathcal{P}, \forall K \in \omega_h \right\}$$
$$\mathcal{X}_h = \left\{ \underline{\underline{\mathcal{M}}}^*_h \in \mathcal{X} \ , \ \underline{\underline{\mathcal{M}}}^*_{h|K} \in \mathcal{P}^3, \forall K \in \omega_h \right\}$$

The semi-discrete in space problem of (4.3) is written:

$$\text{(4.5)} \quad \left\{ \begin{array}{ll} \text{Find } v_{p_h} : [0,T] \to \mathcal{V}_h \text{ and } \underline{\underline{\mathcal{M}}}_h : [0,T] \to \mathcal{X}_h \text{ such that :} & \\ \dfrac{d}{dt} \displaystyle\int_\omega a \rho_p v_{p_h} v^*_{p_h} - h(\underline{\underline{\mathcal{M}}}_h, v^*_{p_h}) = \int_\omega f_p v^*_{p_h}, & \forall v^*_{p_h} \in \mathcal{V}_h, \\ \dfrac{d}{dt} \displaystyle\int_\omega a^{-3} \mathbf{C}^{-1} \underline{\underline{\mathcal{M}}}_h : \underline{\underline{\mathcal{M}}}^*_h + (1 + \eta_p \frac{d}{dt}) h(\underline{\underline{\mathcal{M}}}^*_h, v_{p_h}) = 0, & \forall \underline{\underline{\mathcal{M}}}^*_h, \in \mathcal{X}_h, \end{array} \right.$$

This problem leads to the following matricial differential system after having expanded the unknowns v_{p_h} and $\underline{\underline{\mathcal{M}}}_h$ in a basis of the spaces $\mathcal{V}_h$ and $\mathcal{X}_h$ respectively. For the sake of simplicity, the same notations are used for the vectors v_{p_h} and $\underline{\underline{\mathcal{M}}}_h$ and their coordinates in those particular basis.

$$\text{(4.6)} \quad \left\{ \begin{array}{l} M_h^{v_p} \dfrac{dv_{p_h}}{dt} - H_h^\top \underline{\underline{\mathcal{M}}}_h = f_{p_h} \\ M_h^{\mathcal{M}} \dfrac{d\underline{\underline{\mathcal{M}}}_h}{dt} + (1 + \eta_p \dfrac{d}{dt}) H_h v_p = 0, \end{array} \right.$$

where $M_h^{v_p}$ and $M_h^{\mathcal{M}}$ are positive definite mass matrices. H_h represents a discrete Jacobian operator and $H_h^\top$ its transpose.

Elimination of $\underline{\underline{\mathcal{M}}}_h$. The introduction of the bending moment increases the size of the plate problem since it is a second order tensor. In addition, as presented below the plate equation is solved analytically in time, which requires to calculate the eigenelements of the discretized space-operator. It is of interest to reduce the size of equation (4.6) by eliminating the additional unknown $\underline{\underline{\mathcal{M}}}_h$. This leads to the following equation, obtained by differentiating (4.6a) in time and using (4.6b):

$$\text{(4.7)} \qquad M_h^{v_p} \frac{d^2 v_{p_h}}{dt^2} + 2A_h \frac{dv_{p_h}}{dt} + K_h v_{p_h} = \dot{f}_{p_h}, \quad \forall t \geq 0,$$

where $K_h = H_h^T (M_h^{\mathcal{M}})^{-1} H_h$ and $\dot{f}_{p_h} = \dfrac{df_{p_h}}{dt}$ and $2A_h = \eta_p K_h$.

Choice of $\mathcal{P}$. First, a numerical dispersion analysis shows that a second order approximation of $H^1(\omega)$ reduces significantly the error made on the eigenfrequencies of the soundboard compared to the choice of usual P_1 continuous finite elements (see section 4.3). Second, the computation of K_h requires to invert the positive definite mass matrix $M_h^{\mathcal{M}}$. Therefore, $M_h^{\mathcal{M}}$ is computed approximately with an appropriate quadrature formula, so that it reduces to a 3x3 block diagonal matrix without loss of accuracy This technique called mass lumping [15, 14] permits to invert $M_h^{\mathcal{M}}$ easily. The mass matrix $M_h^{v_p}$ is reduced to a diagonal matrix via the same technique.

It appears that it is not possible to obtain mass lumping with usual P_2 continuous finite elements for the approximation of $H^1(\omega)$ since it leads to an ill posed

problem. We have chosen the following enriched $P_2 \oplus [b]$ continuous finite elements space introduced by Tordjmann *et al.*[15] to circumvent this problem. Thus:

$$\mathcal{P} = P_2 \oplus [b], \tag{4.8}$$

where b denotes the polynomial bubble function of degree 3 defined as follows: let x denote a variable in $\mathbb{R}^2$ and S_1, S_2 and S_3 the vertices of a triangle K. The barycentric coordinates of x with respect to S_1, S_2 and S_3 are denoted $\lambda_1(x), \lambda_2(x)$ and $\lambda_3(x)$ [12]. Then $b(x) = \lambda_1(x)\lambda_2(x)\lambda_3(x)$. The degrees of freedom of $\mathcal{V}_h$ and $\mathcal{X}_h$ are located at the vertices $(S_l)_{1\leq l\leq 3}$, at the gravity center G of each triangle and at the center $(M_l)_{1\leq l\leq 3}$ of each edge, as represented on Fig. 4.1.

(a) $\mathcal{V}_h$ (b) $\mathcal{X}_h$

FIG. 4.1. *Degrees of freedom for $P_2 \oplus [b]$ continuous finite element approximation*

4.3. Dispersion curves of the semi-discretized plate's equation. In the present study, an analysis of the numerical dispersion introduced by Lagrange finite element space approximation of (4.3) of first and second order has been performed. This analysis measures the error made by the approximation scheme on the phase velocity of harmonic plane wave solutions in the homogeneous case for an infinite undamped plate, which shows the consistency of the method in this particular case. One of the interests of this study is that it is a precious indicator which allows to compare the performance of different order finite element approximations. We consider the Kirchhoff-Love's problem for an homogeneous orthotropic undamped plate in $\mathbb{R}^2$:

$$a\rho_p \frac{\partial^2 u_p}{\partial t^2} + \operatorname{div} \underline{\operatorname{Div}}\, a^3 \mathbf{C}\, \underline{\underline{\varepsilon}}(\underline{\nabla} u_p) = 0, \quad \text{in } \mathbb{R}^2. \tag{4.9}$$

Dispersion relation for the continuous problem. We seek for progressive harmonic plane wave solutions of (4.9) of the form:

$$u(\underline{x}, t) = e^{i(\omega t - \underline{k}\cdot\underline{x})} = e^{i(\omega t - k_x x - k_y y)}, \tag{4.10}$$

where $\underline{k} = (k_x, k_y) = (|k|\cos\phi, |k|\sin\phi)$ is the wave vector with propagation direction ϕ and $v_\varphi = w/|k|$ is the phase velocity. Introducing (4.10) in (4.9) gives the velocity phase of plane wave solutions of Kirchhoff-Love's orthotropic plate equation:

$$v_\varphi = \frac{\omega}{|k|} = |k|\, a \sqrt{\frac{c_{11}}{\rho_p}} C(\phi), \tag{4.11}$$

where

$$C(\phi) = \sqrt{\left(\cos^4(\phi) + \tilde{c}_{22}\sin^4(\phi) + 2(\tilde{c}_{12} + \tilde{c}_{33})\cos^2(\phi)\sin^2(\phi)\right)}. \tag{4.12}$$

Note that the plate equation is dispersive, since the phase velocity depends on $|k|$.

Dispersion relation of the semi-discretized scheme. A regular mesh of $\mathbb{R}^2$ made of half square triangles with space step h_p is introduced. The vertex of this mesh are indexed by $(p,q) \in \mathbb{Z}^2$. In the following, we consider the standard first order continuous approximation of $H^1(\mathbb{R}^2)$ based on this mesh, that is $\mathcal{P} = P_1$ and the second order continuous approximation of $H^1(\mathbb{R}^2)$ presented above, that is $\mathcal{P} = P_2 \oplus [b]$ For a given wave vector $\underline{k}$, we seek for the phase velocity v_{φ_h} of discrete harmonic plane wave solutions of these two semi-discretized schemes, of the form:

$$u_h(ph_p, qh_p, t) = e^{(i\omega_h t - ik_x ph_p - ik_y qh_p)}, \quad \forall p, q \in \mathbb{Z}, \tag{4.13}$$

The error made on the phase velocity is measured by the ratio between the continuous phase velocity and the discrete one:

$$q_h = \frac{v_{\varphi_h}}{v_\varphi} = \frac{\omega_h}{\omega}.$$

It can be shown that q_h is a function of the propagation angle ϕ and of the inverse of number of points per wave length $K = \frac{|k|h}{2\pi}$, that is $q_h = q_h(K, \phi)$ [17, 14].

Dispersion curves. For a fixed propagation angle ϕ, the curve $K \mapsto q_h(K, \phi)$ shows the accuracy of the scheme versus the refinement of the mesh. The closer to 1 the curve, the more accurate the scheme. These curves are plotted for the approximations of first and second order on Fig. 4.2. Typical values of wood orthotropy are taken (see Table. 7.1), but the results are similar with other values of orthotropy.

The error made on the phase velocity is far greater with the first order scheme. For example, for the first order scheme, the error made on the phase velocity is less than 10% with nearly 7 points per wave length ($K \approx 0.15$). For the second order approximation, this correspond to $K \approx 0.30$, since the number of degrees of freedom is approximately twice greater for the same value of K. But only 2 points per wave length are enough ($K = 0.5$) with the second order scheme to obtain the same accuracy. This analysis justifies thus the choice of a second order scheme.

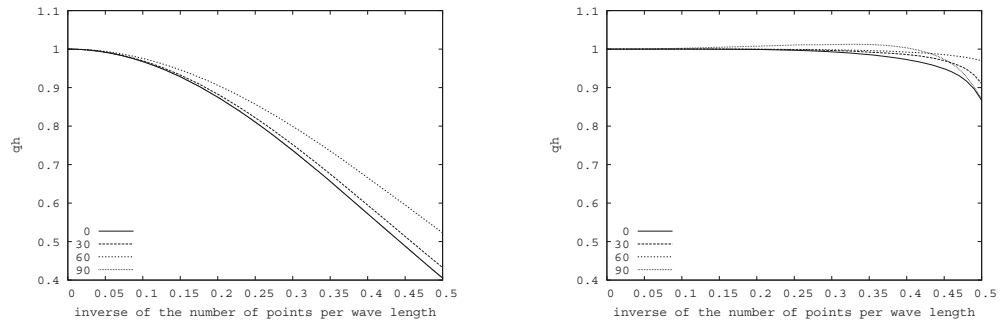

(a) First order

(b) Second order

FIG. 4.2. *Error made on the phase velocity with the semi-discrete approximation, $K \mapsto q_h(K, \phi)$ for the angles of propagation ϕ = 0, 30, 60 and 90 degrees.*

4.4. Time discretization. In this section, three different strategies for the time discretization of the spatial semi-discretized scheme (4.7) are investigated: explicit finite differences, implicit finite differences and analytical resolution in time. A standard approach for the time resolution of (4.7) is the use of finite differences, in order

to minimize the computation cost at each time step. As explained below, it appears that for both precision and efficiency reasons, the use of a finite differences scheme is not well suited for the plate equation, neither explicit, nor implicit. Therefore, the spatial semi-discretized problem is solved exactly in time.

Explicit scheme. Given a time step Δt and for an undamped plate, the simplest time resolution of (4.7) consists of using the standard leapfrog scheme. The stability of this scheme is guaranteed under a so called CFL condition. In order to quantify this condition, a Fourier analysis in the homogeneous case for an infinite plate of space step h_p is realized. In this case, it can be shown that for a second order scheme ($\mathcal{P} = P_2 \oplus [b]$) and for typical values of wood orthotropy (see Table. 7.1), the stability condition of a standard explicit centered finite difference scheme of second order in time of (4.7) is (see [17]):

$$\alpha = a\sqrt{\frac{c_{11}}{\rho_p}}\frac{\Delta t}{h_p^2} \leq 0.084880 = \alpha_0. \tag{4.14}$$

In practice, with parameters values used in the numerical experiments, this condition would impose to choose $\Delta t \approx 8.4\,10^{-7}s$. Consequently, the number of iterations is very high, even for very short duration experiment. For this reason, the explicit scheme cannot be used, in particular in view of the coupling of the plate to the 3D acoustic equation. In addition, when the dissipative term of viscoelastic type is not zero, it is not possible to write a stable centered finite difference scheme any more. In this case the scheme becomes necessary *implicit*, which arises the cost of this method.

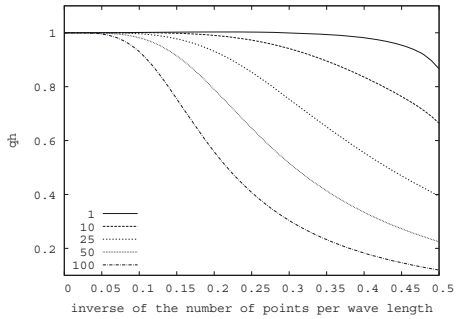

FIG. 4.3. *Error made on the phase velocity with the second order approximation in space and an implicit scheme in time.* $\phi = 0$ *and* $\alpha = C\alpha_0$ *with* C *= 1, 10, 25, 50, 100*

Implicit scheme. A first idea to circumvent this problem would be to use an implicit unconditionally stable scheme, as it is usually done for the heat equation, allowing greater time steps, and also allowing the introduction of dissipative terms without additional cost. However, since the solution has to be computed for long times, and consequently for a great number of iterations, the inversion of a matrix at each time step is in itself very costly. Furthermore, a numerical dispersion analysis similar to the one presented in section (4.3) has been realized to give indications in the choice of the time step Δt. This analysis shows that the time step must be chosen sufficiently small for efficiency considerations. More precisely, we consider a standard implicit centered finite difference scheme of second order in time of (4.7). Given a wave vector $\underline{k}$, we seek for the phase velocity $v^I_{\varphi_h}$ of discrete harmonic plane wave solutions of this implicit scheme, of the form:

$$u_h(ph_p, qh_p, n\Delta t) = e^{(i\omega_h^I n\Delta t - ik_x ph_p - ik_y qh_p)}, p, q \in \mathbb{Z}, \tag{4.15}$$

It can be shown that the error made on the phase velocity, denoted q_h^I, verifies $q_h^I = q_h^I(K, \phi, \alpha)$, where K and ϕ are defined in section (4.3) and α is defined in (4.14) [17]. Figure 4.3 shows the error made on the phase velocity by the implicit scheme for the $P_2 \oplus [b]$ finite element approximation, for a fixed angle of propagation $\phi = 0°$ and for various values of α such that $\alpha = C\alpha_0$ with $C \in \{1, 10, 25, 50, 100\}$ (α_0 is defined in (4.14)). The curve obtained for $\alpha = \alpha_0$ and the dispersion curve of the semi-discrete problem are the same.

These curves show that the error made on the phase velocity decreases rapidly for increasing values of α, which means that the effienciency of the implicit scheme degrades significantly for large α. Consequently, in order to keep the accuracy of the space approximation, it appears that Δt has to be proportional to h_p^2, as for the explicit scheme. Even if this solution allows greater values of Δt, this condition is still too restrictive, and for this reason, the implicit scheme cannot be used.

Analytical resolution. The idea retained in this study to cope with this problem is to solve (4.7) analytically in time, which allows to choose any Δt without degrading the accuracy of the spatial semi-discretized scheme. In practice, it is necessary to sample the solution in time in order to compute it. Thus, given a time step Δt, v_{p_h} and $\dot{v}_{p_h} = \dfrac{dv_{p_h}}{dt}$ are computed at times $t^{n+\frac{1}{2}} = (n + \frac{1}{2})\Delta t$ and (4.7) is solved on each interval $[t^{n-\frac{1}{2}}, t^{n+\frac{1}{2}}]$. In the guitar problem, f_{p_h} represent the effort exerted by the string and the air in the complete guitar problem. Since the string and acoustic equations are solved by finite differences with time step Δt, the right hand side is supposed to be constant on the interval $[t^{n-\frac{1}{2}}, t^{n+\frac{1}{2}}]$, and it is given by $\dot{f}_{p_h}^n = f_{p_h}(t^n)$. The following equation is thus solved at each time step:

$$\text{(4.16)} \qquad \begin{cases} M_h^{v_p} \dfrac{d^2 v_{p_h}}{dt^2} + 2A_h \dfrac{dv_{p_h}}{dt} + K_h v_{p_h} = \dot{f}_{p_h}^n, & \forall t \in]t^{n-\frac{1}{2}}, t^{n+\frac{1}{2}}[, \\ v_{p_h}(t^{n-\frac{1}{2}}) = v_{p_h}^{n-\frac{1}{2}} \text{ and } \dot{v}_{p_h}(t^{n-\frac{1}{2}}) = \dot{v}_{p_h}^{n-\frac{1}{2}}, \end{cases}$$

The resolution of this equation is based on the computation of the eigenmodes of the positive matrix K_h. It is given by:

$$\text{(4.17)} \qquad \begin{cases} v_{p_h}^{n+\frac{1}{2}} = \mathcal{S}_{\Delta t}(v_{p_h}^{n-\frac{1}{2}}, \dot{v}_{p_h}^{n-\frac{1}{2}}) + \mathcal{R}_{\Delta t}(\dot{f}_{p_h}^n) \\ \dot{v}_{p_h}^{n+\frac{1}{2}} = \dot{\mathcal{S}}_{\Delta t}(v_{p_h}^{n-\frac{1}{2}}, \dot{v}_{p_h}^{n-\frac{1}{2}}) + \dot{\mathcal{R}}_{\Delta t}(\dot{f}_{p_h}^n), \end{cases}$$

where one has formally, for $v_0, v_1, f \in \mathcal{V}$ and $t > 0$:

$$\text{(4.18)} \qquad \begin{cases} \mathcal{S}_t(v_0, v_1) = \exp(-A_h t) \left[\cos(\tilde{K}_h t) v_0 + \dfrac{\sin(\tilde{K}_h t)}{\tilde{K}_h} (v_1 + A_h v_0) \right] \\ \mathcal{R}_t(f) = \dfrac{1}{2K_h^2 \tilde{K}_h} \left[\tilde{K}_h \big(I - \exp(-A_h t) \cos(\tilde{K}_h t) \big) - A_h \sin(\tilde{K}_h t) \right] \end{cases}$$

where $\tilde{K}_h = \sqrt{K_h - A_h^2}$ [1], $\dot{\mathcal{S}}_t(v_0, v_1) = \dfrac{d\mathcal{S}_t}{dt}(v_0, v_1)$ and $\dot{\mathcal{R}}_t(f) = \dfrac{d\mathcal{R}_t}{dt}(f)$. In the following, for the sake of simplicity, the operators $\mathcal{S}_{\Delta t}$ and $\mathcal{R}_{\Delta t}$ will be denoted $\mathcal{S}$ and $\mathcal{R}$ respectively

[1] the square root is chosen with positive imaginary part for negative arguments

The cost of this analytical scheme is obviously related to the computation of the eigenvalues and eigenvectors of K_h, which is made with the help of a QMR algorithm. But at each time step, the computations are costless so that this scheme is efficient for long duration numerical experiments, as it is the case in sound synthesis problems. In addition, because the frequency spectrum of the excitation f_{p_h} is band-limited, it is not necessary to keep all eigenmodes of K_h, but only the first ones. As an example, in the case of the guitar problem, 50 modes of the plate were used, which correspond to a cut-off frequency nearly equal to 3kHz. Thus, this method is in fact a spectral method for which the modes of the plate are computed using an adapted mixed finite element method. The efficiency of the analytical resolution in time of (4.7) compared to the explicit and implicit finite differences schemes is illustrated by numerical experiments in [17].

5. Numerical resolution of the guitar problem. The space discretization of $\mathcal{P}_g$ is based on a mixed variational formulation of the coupled problem. One has to propose a variational formulation which is adapted to the one chosen for the resolution of the plate equation described in the previous section. A fictitious domain method for the fluid-structure interaction problem is presented (section (5.1)) and a dual mixed velocity-stress mixed formulation for the string is proposed (section (5.2)).

5.1. The fluid-structure interaction: fictitious domain formulation. The fluid-structure interaction problem is obviously the limiting part of the simulation since it is a 3D problem posed in a domain of complex geometry. The finite element method is a usual way to approximate the shape of the instrument with good accuracy. But it leads to a very expensive scheme, both in memory and time, because it is based on a tetrahedral mesh of the domain $\Omega = \mathbb{R}^3 \setminus \Gamma$. On the other hand, the finite difference method, based on a regular mesh, is certainly more efficient, but it leads to a lower order staircase approximation of the instrument.

The interest of the fictitious domain method is that the geometry of the instrument is 'ignored' in some sense. As a consequence, the acoustic pressure and acoustic velocity can be extended in all $\mathbb{R}^3$, and are not only defined in $\mathbb{R}^3 \setminus \Gamma$. Therefore, this method allows to use a regular mesh, made of small cubes, for solving the acoustic equation, which leads in practice to an efficient centered second order finite difference approximation. The condition on the boundary of the guitar is then taken into account in a weak way via the introduction of a Lagrange multiplier λ which appears to be the pressure jump across the surface of the instrument. The discretization of λ relies on a triangular mesh of the surface Γ of the instrument, which leads thus to a good approximation of the geometry. This method has been introduced for the resolution of elliptic problems about thirty years ago [3, 2, 36]. It has been developed more recently by R. Glowinski, Y. Kuznetsov [28, 32] and generalized to evolution problems [27, 34, 7]. In the present study, it is adapted from works on the numerical simulation of the kettledrum by Rhaouti *et al.*[37].

In order to define an extension of the acoustic pressure and velocity to $\mathbb{R}^3$, p and $\underline{\mathbf{v}}_a$ are sought in functional spaces to be determined and denoted $\mathcal{P}$ and $\mathcal{W}$ respectively. The fictitious domain formulation requires that the continuity of the normal component of the velocity involved in the fluid-structure interaction problem is included as an essential condition in $\mathcal{W}$, *ie.*:

$$\forall \underline{\mathbf{v}}_a^* \in \mathcal{W}, [\underline{\mathbf{v}}_a^*]|_\Gamma = 0. \tag{5.1}$$

The spaces $\mathcal{P}$ and $\mathcal{W}$ will be determined from the following variational formulation of (2.3). Equation (2.3a) is multiplied by a test function $\underline{\mathbf{v}}_a^* \in \mathcal{W}$ and (2.3b) is multiplied

by a test function $p^* \in \mathcal{P}$ and integrated on Ω using the Green formula and (5.1):

$$\left\{\begin{array}{ll} \dfrac{d}{dt}\displaystyle\int_{\mathbb{R}^3\setminus\Gamma} \underline{\mathbf{v}}_a \cdot \underline{\mathbf{v}}_a^* - \int_{\mathbb{R}^3\setminus\Gamma} p \operatorname{div} \underline{\mathbf{v}}_a^* - \int_\Gamma [p]_\Gamma (\underline{\mathbf{v}}_a^* \cdot \underline{\mathbf{N}}) = 0, & \forall \underline{\mathbf{v}}_a^* \in \mathcal{W}, \\ \dfrac{d}{dt}\displaystyle\int_{\mathbb{R}^3\setminus\Gamma} pp^* + \int_{\mathbb{R}^3\setminus\Gamma} p^* \operatorname{div} \underline{\mathbf{v}}_a = 0, & \forall p^* \in \mathcal{P}, \end{array}\right. \tag{5.2}$$

In order to avoid the construction of a tetrahedral mesh of $\mathbb{R}^3 \setminus \Gamma$ needed for the computation of the pressure jump, the new unknown $\lambda = [p]_\Gamma$ is introduced. Also, for the same reasons, the boundary conditions on Γ (2.3c-d) are written in a weak way. Multiplying (2.3c) and (2.3d) by a test function $\lambda^* \in \mathcal{L}$, and integrating on ω and on Σ respectively yields:

$$\int_\omega v_p \lambda^*_{|\omega} - \int_\Gamma \lambda^* (\underline{\mathbf{v}}_a \cdot \underline{\mathbf{N}}) = 0, \quad \forall \lambda^* \in \mathcal{L}. \tag{5.3}$$

The variational formulation (5.2, 5.3) imposes to p and p^* to be in $L^2(\mathbb{R}^3 \setminus \Gamma)$ which can be naturally extended to $L^2(\mathbb{R}^3)$, since Γ is a surface. On the other hand this formulation imposes to $\underline{\mathbf{v}}_a$ and $\underline{\mathbf{v}}_a^*$ to be in $H(\operatorname{div}, \mathbb{R}^3 \setminus \Gamma)$ which is naturally extended to $H(\operatorname{div}, \mathbb{R}^3)$ by continuity of the normal component on Γ (5.1), introduced in the space $\mathcal{W}$. In addition, λ and λ^* are chosen in $H^{1/2}_{00}(\Gamma)$ in order to give sense to the weak formulation (5.3). Finally, the fictitious formulation of (2.3) is given by:

$$\left\{\begin{array}{ll} \text{Find } p : [0,T] \to \mathcal{P},\ \underline{\mathbf{v}}_a : [0,T] \to \mathcal{W},\ \text{et } \lambda : [0,T] \to \mathcal{L},\ \text{such that:} & \\ \dfrac{d}{dt}\displaystyle\int_{\mathbb{R}^3} \rho_a \underline{\mathbf{v}}_a \cdot \underline{\mathbf{v}}_a^* - \int_{\mathbb{R}^3} p \operatorname{div} \underline{\mathbf{v}}_a^* - \langle \underline{\mathbf{v}}_a^* \cdot \underline{\mathbf{N}}, \lambda \rangle_\Gamma = 0, & \forall \underline{\mathbf{v}}_a^* \in \mathcal{W}, \\ \dfrac{d}{dt}\displaystyle\int_{\mathbb{R}^3} \mu_a pp^* + \int_{\mathbb{R}^3} p^* \operatorname{div} \underline{\mathbf{v}}_a = 0, & \forall p^* \in \mathcal{P}, \\ \displaystyle\int_\omega v_p \lambda^* - \langle \underline{\mathbf{v}}_a \cdot \underline{\mathbf{N}}, \lambda^* \rangle_\Gamma = 0, & \forall \lambda^* \in \mathcal{L}. \end{array}\right. \tag{5.4}$$

where $\langle ., . \rangle_\Gamma$ denotes the duality bracket defined on $H^{-\frac{1}{2}}(\Gamma) \times H^{\frac{1}{2}}(\Gamma)$ and:

$$\mathcal{P} = L^2(\mathbb{R}^3), \quad \mathcal{W} = H(\operatorname{div}, \mathbb{R}^3), \quad \mathcal{L} = H^{\frac{1}{2}}_{00}(\Gamma). \tag{5.5}$$

5.2. String equation. In order to simplify the presentation, the dissipative viscoelastic term η_s is supposed to be zero. It does not add formal difficulty to take into account this damping term in the numerical resolution proposed here [17]. The coupling terms at the bridge involve a Dirichlet condition (2.1c) and a Neumann one (2.5). A dual mixed formulation of the string equation has been chosen, using the velocity $v_s = \partial_t u_s$ and the stress $q = T \partial_x u_s$. Equation (2.1) is thus rewritten in the following equivalent form of first order in time and first order in space:

$$\left\{\begin{array}{lll} (a) & \rho_s \partial_t v_s - \partial_x q = f_s, & \text{in }]0, l_s[, \\ (b) & \partial_t q - T \partial_x v_s = 0, & \text{in } \in]0, l_s[, \\ (c) & v_s(0,t) = 0, & \forall t > 0, \\ (d) & v_s(l_s,t) = \displaystyle\int_\omega G v_p, & \forall t > 0, \end{array}\right. \tag{5.6}$$

The variational formulation of (5.6) is obtained by multiplying equation (5.6a) by a test function v_s^* and integrating on $]0, l_s[$. Then (5.6b) is multiplied by a test function q^* and integrated by part on $]0, l_s[$, which yields, using the conditions (5.6c-d):

$$
\left\{
\begin{array}{l}
\text{Find } v_s : [0,T] \to \mathcal{U}, \text{ and } q : [0,T] \to \mathcal{Q}, \\
\dfrac{d}{dt}\displaystyle\int_0^{l_s} \rho_s v_s v_s^* - \int_0^{l_s} v_s^* \partial_x q = \int_0^{l_s} f_s v_s^*, \qquad \forall v_s^* \in \mathcal{U}, \\
\dfrac{d}{dt}\displaystyle\int_0^{l_s} \frac{1}{T} q q^* + \int_0^{l_s} v_s \partial_x q^* - q^*(l_s,t)\int_\omega G v_p = 0, \quad \forall q^* \in \mathcal{Q},
\end{array}
\right. \tag{5.7}
$$

where $\mathcal{U} = L^2(]0, l_s[)$ and $\mathcal{Q} = H^1(]0, l_s[)$. In this way, the boundary condition (2.1c) becomes natural and does not couple the functional spaces related to the plate and the functional spaces related to the string, which simplifies the spatial approximation of the coupled problem.

5.3. Variational formulation of the complete problem. The force f_p exerted on the plate by the surrounding air and by the string is rewritten with the new variables λ and q introduced above:

$$
f_p(x,y,t) = -q(l_s,t)G(x,y) - \lambda_{|\omega}, \tag{5.8}
$$

The results of section 4 are transposed without difficulty. The complete variational formulation of problem $\mathcal{P}_g$ is finally given by the set of equations (4.3, 5.4, 5.7, 5.8).

5.4. Space approximation. In order to write a conforming approximation of the variational formulation (4.3, 5.4, 5.7, 5.8), the following finite dimensional spaces are introduced:

$$
\mathcal{U}_h \subset \mathcal{U}, \quad \mathcal{Q}_h \subset \mathcal{Q}, \quad \mathcal{V}_h \subset \mathcal{V}, \quad \mathcal{X}_h \subset \mathcal{X}, \quad \mathcal{W}_h \subset \mathcal{W}, \quad \mathcal{P}_h \subset \mathcal{P}, \quad \mathcal{L}_h \subset \mathcal{L}.
$$

The semi-discretized in space problem is written:

(5.9)

$$
\left\{
\begin{array}{l}
\text{Find } v_{s_h} : [0,T] \to \mathcal{U}_h,\ q_h : [0,T] \to \mathcal{Q}_h,\ v_{p_h} : [0,T] \to \mathcal{V}_h,\ \underline{\underline{\mathcal{M}}}_h : [0,T] \to \mathcal{X}_h, \\
\qquad p_h : [0,T] \to \mathcal{P}_h,\ \underline{\mathbf{v}}_{a_h} : [0,T] \to \mathcal{W}_h, \text{ and } \lambda : [0,T] \to \mathcal{L}_h, \text{ such that :} \\
\dfrac{d}{dt}\displaystyle\int_0^{l_s} \rho_s v_{s_h} v_{s_h}^* - \int_0^{l_s} \partial_x q_h v_{s_h}^* = \int_0^{l_s} f_s v_{s_h}^*, \qquad \forall v_{s_h}^* \in \mathcal{U}_h, \\
\dfrac{d}{dt}\displaystyle\int_0^{l_s} \frac{1}{T} q_h q_h^* + \int_0^{l_s} \partial_x q_h^* v_{s_h} - q_h^*(l_s,t)\int_\omega G v_{p_h} = 0 \qquad \forall q_h^* \in \mathcal{Q}_h, \\
\dfrac{d}{dt}\displaystyle\int_\omega \rho_p v_{p_h} v_{p_h}^* - h(v_{p_h}^*, \underline{\underline{\mathcal{M}}}_h) = -q_h(l_s,t)\int_\omega G v_{p_h}^* - \int_\omega v_{p_h}^* \lambda_h, \quad \forall v_{p_h}^* \in \mathcal{V}, \\
\dfrac{d}{dt}\displaystyle\int_\omega a^{-3}\mathbf{C}^{-1}\,\underline{\underline{\mathcal{M}}}_h : \underline{\underline{\mathcal{M}}}_h^* + (1+\eta_p\frac{d}{dt})h(\underline{\underline{\mathcal{M}}}_h^*, v_{p_h}) = 0, \qquad \forall \underline{\underline{\mathcal{M}}}_h^*, \in \mathcal{X}_h, \\
\dfrac{d}{dt}\displaystyle\int_{\mathbb{R}^3} \rho_a \underline{\mathbf{v}}_{a_h} \cdot \underline{\mathbf{v}}_{a_h}^* - \int_{\mathbb{R}^3} p_h \operatorname{div} \underline{\mathbf{v}}_{a_h}^* - \langle \underline{\mathbf{v}}_{a_h}^* \cdot \underline{\mathbf{N}}, \lambda_h \rangle_\Gamma = 0, \qquad \forall \underline{\mathbf{v}}_{a_h}^* \in \mathcal{W}_h, \\
\dfrac{d}{dt}\displaystyle\int_{\mathbb{R}^3} \mu_a p_h p_h^* + \int_{\mathbb{R}^3} p_h^* \operatorname{div} \underline{\mathbf{v}}_{a_h} = 0, \qquad \forall p_h^* \in \mathcal{P}_h, \\
\displaystyle\int_\omega v_{p_h} \lambda_h^* - \langle \underline{\mathbf{v}}_{a_h} \cdot \underline{\mathbf{N}}, \lambda_h^* \rangle_\Gamma = 0. \forall \lambda_h^* \in \mathcal{L}_h.
\end{array}
\right.
$$

A basis of each of the finite dimensional spaces defined above is introduced. This problem leads to the following matricial differential system after having eliminated the bending moment $\underline{\underline{\mathcal{M}}}_h$ as described in section (4.2). For the sake of simplicity, the same notations are used: $(v_{s_h}, q_h, \underline{\mathbf{v}}_{a_h}, p_h, \lambda_h)$ denote now the vectors of coordinates of the unknowns in the standard finite element bases and v_{p_h} denote the vector of modal components of the spatial approximation of the plate velocity.

$$
\left\{
\begin{array}{ll}
(a) & M_h^{v_s} \dfrac{dv_{s_h}}{dt} - D_h q_h = f_{s_h}, \\
(b) & M_h^{q} \dfrac{dq_h}{dt} + D_h^\top v_{s_h} - J_h^\top v_{p_h} = 0, \\
(c) & M_h^{v_p} \dfrac{d^2 v_{p_h}}{dt^2} + 2A_h \dfrac{dv_{p_h}}{dt} + K_h v_{p_h} = -J_h \dfrac{dq}{dt}_h - B_{\omega_h}^\top \dfrac{d\lambda_h}{dt}, \\
(d) & M_h^{v_a} \dfrac{d\underline{\mathbf{v}}_{a_h}}{dt} - G_h p_h - B_{\Gamma_h}^\top \lambda_h = 0, \\
(e) & M_h^{p} \dfrac{dp_h}{dt} + G_h^\top \underline{\mathbf{v}}_{a_h} = 0, \\
(f) & B_{\omega_h} v_{p_h} - B_{\Gamma_h} \underline{\mathbf{v}}_{a_h} = 0,
\end{array}
\right. \tag{5.10}
$$

where $A^\top$ denotes the transpose of a matrix A. $M_h^{v_s}$, M_h^{q}, $M_h^{v_p}$, $M_h^{\mathcal{M}}$, $M_h^{v_a}$ and M_h^{p} are positive definite mass matrices. The matrix D_h represents a discrete 1D divergence, its transpose a discrete 1D gradient. The matrix K_h represents the Kirchhoff-Love plate operator and is defined by (4.7). The matrix A_h represents the damping effects in the plate and is defined by $2A_h = \eta_p K_h$. The matrix G_h is a discrete 3D gradient operator and its transpose a discrete 3D divergence. The matrices J_h, B_{ω_h} and B_{Γ_h} represent discrete trace operators which couple the unknowns plate to the string and to the air. Finally f_{s_h} represents a space approximation of the string excitation f_s.

Discrete energy identity. It is easy to show the following energy identity of the semi-discretized in space problem. This identity is a semi-discrete version of the continuous one given in (3.3) after having differentiated in time all the unknowns. This is a consequence of the particular resolution of the plate-string coupling, which imposes to work with the variables v_s, q and v_p.

THEOREM 5.1 (Energy identity of the semi discretized problem). *The solution of (5.10) satisfies:*

$$
\frac{dE_h}{dt}(t) = (\frac{df_{s_h}}{dt}, \frac{dv_{s_h}}{dt}) - \|\frac{dv_{p_h}}{dt}\|^2_{A_h} \tag{5.11}
$$

where E_h is defined by:

(5.12)

$$
E_h(t) = \frac{1}{2}\|\frac{dv_{s_h}}{dt}\|^2_{M_h^{v_s}} + \frac{1}{2}\|\frac{dq_h}{dt}\|^2_{M_h^{q}} + \frac{1}{2}\|\frac{dv_{p_h}}{dt}\|^2 + \frac{1}{2}\|v_{p_h}\|^2_{K_h} + \frac{1}{2}\|\frac{d\underline{\mathbf{v}}_{a_h}}{dt}\|^2_{M_h^{v_a}} + \frac{1}{2}\|\frac{dp}{dt}\|^2_{M_h^{p}}.
$$

and where for any positive definite matrix M, $\|.\|_M$ denotes the norm associated to the scalar product on R^n defined by $(U,V)_M = (U, MV), \forall U, V \in \mathbb{R}^n$.

Approximation spaces for the string equation. A standard approximation of lower order is used. A regular mesh of the string with segments of size h_s is given. Then:

- $L^2(]0, l_s[)$ is approximated with P_0 discontinuous finite elements. The degrees of freedom (dof) are located at the middle of each segment.

- $H^1(]0, l_s[)$ is approximated with P_1 continuous finite elements. The degrees of freedom are located at the vertex of each segment.

The mass matrices $M_h^{v_s}$ is diagonal in the standard finite element basis of $\mathcal{U}_h$. M_h^q is reduced to diagonal using standard mass lumping technique. With this choice, the obtained scheme can be interpreted as a standard lower order centered finite difference approximation of the 1D divergence operator. By definition of Lagrange P_1 continuous functions, all basis function of $\mathcal{Q}_h$ are zero at the bridge, that is at the point $x = l_s$, except the one associated to the last node. Thus only the last column of J_h is not zero. This last property will be helpful for the resolution algorithm of the discretized scheme of the complete problem (see section (5.5.2)).

Approximation spaces for the plate equation. $P_2 \oplus [b]$ continuous finite element associated with a triangular mesh of ω, described in section (4.2), are used for the approximation of $H^1(\omega)$ and $(H^1(\omega))^3$.

Approximation spaces for the fluid-structure interaction equations. It is not possible to approximate the spaces $L^2(\mathbb{R}^3)$ and $H(\mathrm{div}, \mathbb{R}^3)$, since $\mathbb{R}^3$ is unbounded. Therefore, the computation domain is artificially bounded by the use of Absorbing Boundary Conditions introduced by Engquist *et al.*[21]. In the present study, higher order ABC proposed by Collino [16] were used, essentially for their implementation simplicity. The computations are thus restricted to a box of finite size denoted $\mathcal{C}$.

The basic principle of this method consists of adding artificial absorbing conditions on the boundaries of the computational domain. More precisely, it is possible to define exactly transparency conditions in the frequency domain. These conditions are approximated with higher order Padé approximation, in order to obtain local boundary conditions both in space and time. For the sake of simplicity, these boundary conditions are not presented in this paper. For more details, see [16, 37].

A regular mesh of $\mathcal{C}$ made with cubes of size h_a and a triangular mesh Γ_h of the guitar of step size h_λ are introduced. Then:

- $H(\mathrm{div}, \mathcal{C})$ is approximated with standard lower order mixed finite elements of Raviart-Thomas, associated to the regular mesh of $\mathcal{C}$,
- $L^2(\mathcal{C})$ is approximated with Q_0 discontinuous finite elements, associated to the regular mesh of $\mathcal{C}$,
- $H_{00}^{\frac{1}{2}}(\Gamma)$ is approximated with P_1 continuous finite elements, associated to the mesh Γ_h.

The degrees of freedom for $\underline{\mathbf{v}}_{a_h}$, p_h and λ_h are represented on Fig. 5.1

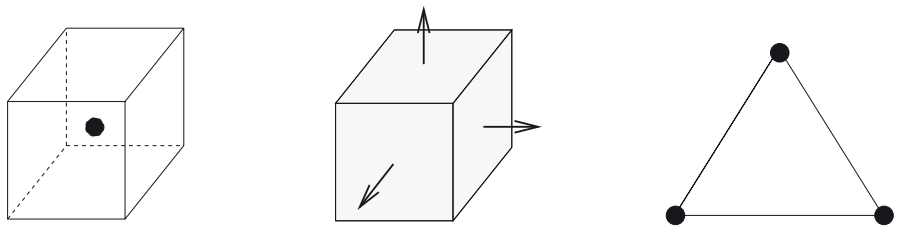

FIG. 5.1. *Degrees of freedom for the approximation of $L^2(\mathcal{C})$ (a) and $H(\mathrm{div}, \mathcal{C})$ (b) on a regular cubic mesh of $\mathcal{C}$ and for the approximation of $H_{00}^{\frac{1}{2}}(\Gamma)$ on a triangular mesh of Γ.*

The mass matrices M_h^p is diagonal in the standard finite element basis of $\mathcal{P}_h$.

$M_h^{v_a}$ is reduced to diagonal using standard mass lumping technique. With this choice, the obtained scheme can be interpreted as a standard lower order centered finite difference approximation of the 3D gradient operator.

5.5. Time discretization.

5.5.1. The numerical scheme. For the time discretization, a constant time step Δt is chosen. A centered finite difference scheme is used for the string and for the air while the plate equation is solved exactly in continuous time as described in section (4.4). This scheme is written in such a way that almost all computations are *explicit*, in particular for the 3D part. Therefore, the unknowns $v_{p_h}, \dot{v}_{p_h}, v_{s_h}$ and p_h are computed at instants $t^{n+\frac{1}{2}}$ while q_h and $\underline{\mathbf{v}}_{a_h}$ are computed at instant t^n. In addition, this scheme is chosen is order to be able to derive a fully discrete energy identity. In this aim a conservative time approximation of the coupling terms leads to choose two different centered schemes for the approximation of $\frac{dq_h}{dt}$ and $\frac{d\lambda_h}{dt}$ in (5.10c). The following scheme for the time resolution of (5.10c) is proposed:

(5.13)
$$\begin{cases} \ddot{v}_{p_h} + 2A_h\dot{v}_{p_h} + K_h v_{p_h} = -J_h\dfrac{q_h^{n+1}-q_h^{n-1}}{2\Delta t} - B_{\omega_h}^\top \dfrac{\lambda_h^{n+\frac{1}{2}}-\lambda_h^{n-\frac{1}{2}}}{\Delta t}, \forall t \in]t^{n-\frac{1}{2}}, t^{n+\frac{1}{2}}[, \\ v_{p_h}(t^{n-\frac{1}{2}}) = v_{p_h}^{n-\frac{1}{2}} \text{ and } \dot{v}_{p_h}(t^{n-\frac{1}{2}}) = \dot{v}_{p_h}^{n-\frac{1}{2}}, \end{cases}$$

This constraint leads also to discretize (5.10f) differentiated in time as it will be shown in the proof of theorem 6.1. Finally, using (4.17) for the resolution of (5.13) the following scheme is obtained:

(5.14)
$$\begin{cases} (a) \quad M_h^{v_s}\dfrac{v_{s_h}^{n+\frac{1}{2}}-v_{s_h}^{n-\frac{1}{2}}}{\Delta t} - D_h q_h^n = f_{s_h}^n, \\ (b) \quad M_h^q\dfrac{q_h^{n+1}-q_h^n}{\Delta t} + D_h^\top v_{s_h}^{n+\frac{1}{2}} - J_h^\top v_{p_h}^{n+\frac{1}{2}} = 0, \\ (c) \quad v_{p_h}^{n+\frac{1}{2}} = \mathcal{S}(v_{p_h}^{n-\frac{1}{2}}, \dot{v}_{p_h}^{n-\frac{1}{2}}) - \mathcal{R}B_{\omega_h}^\top(\dfrac{\lambda_h^{n+\frac{1}{2}}-\lambda_h^{n-\frac{1}{2}}}{\Delta t}) - \mathcal{R}J_h(\dfrac{q_h^{n+1}-q_h^{n-1}}{2\Delta t}) \\ (d) \quad \dot{v}_{p_h}^{n+\frac{1}{2}} = \dot{\mathcal{S}}(v_{p_h}^{n-\frac{1}{2}}, \dot{v}_{p_h}^{n-\frac{1}{2}}) - \dot{\mathcal{R}}B_{\omega_h}^\top(\dfrac{\lambda_h^{n+\frac{1}{2}}-\lambda_h^{n-\frac{1}{2}}}{\Delta t}) - \dot{\mathcal{R}}J_h(\dfrac{q_h^{n+1}-q_h^{n-1}}{2\Delta t}), \\ (e) \quad M_h^{v_a}\dfrac{\underline{\mathbf{v}}_{a_h}^{n+1}-\underline{\mathbf{v}}_{a_h}^n}{\Delta t} - G_h p_h^{n+\frac{1}{2}} - B_{\Gamma_h}^\top \lambda_h^{n+\frac{1}{2}} = 0, \\ (f) \quad M_h^p\dfrac{p_h^{n+\frac{1}{2}}-p_h^{n-\frac{1}{2}}}{\Delta t} + G_h\underline{\mathbf{v}}_{a_h}^n = 0, \\ (g) \quad B_{\omega_h}\dfrac{v_{p_h}^{n+\frac{1}{2}}-v_{p_h}^{n-\frac{1}{2}}}{\Delta t} - B_{\Gamma_h}\dfrac{\underline{\mathbf{v}}_{a_h}^{n+1}-\underline{\mathbf{v}}_{a_h}^{n-1}}{2\Delta t} = 0. \end{cases}$$

5.5.2. Resolution algorithm of the scheme. The practical resolution of the scheme (5.14) has to be explained. We seek for ($v_{s_h}^{n+\frac{1}{2}}$, q_h^{n+1}, $v_{p_h}^{n+\frac{1}{2}}$, $\dot{v}_{p_h}^{n+\frac{1}{2}}$, $\underline{\mathbf{v}}_{a_h}^{n+1}$, $p_h^{n+\frac{1}{2}}$, $\lambda_h^{n+\frac{1}{2}}$), all other terms being known at this step of the computations. In this system, notice that (5.14d) is simply (5.14c) differentiated in time, so that these 2 equations are redundant. In fact, $\dot{v}_{p_h}^{n+\frac{1}{2}}$ should only be computed in order to know the initial conditions at the next step.

Since the mass matrices $M_h^{v_s}$ and M_h^p are diagonal, (5.14a) and (5.14f) give explicitly $v_{s_h}^{n+\frac{1}{2}}$ and $p_h^{n+\frac{1}{2}}$. Then, since only the last column of the matrix J_h is not zero (see section (5.4)), it is possible to uncouple the last component of the vector q_h^{n+1}, which corresponds to the dof associated to the bridge. Therefore, we denote:

$$q_h^{n+1} = (\bar{q}_h^{n+1}, Q_h^{n+1}) \in \mathbb{R}^{n_q-1} \times \mathbb{R}, \tag{5.15}$$

and similar notations for M_h^q and D_h. Equation (5.14b) can be rewritten:

$$\begin{cases} (a) \quad \bar{M}_h^q \dfrac{\bar{q}_h^{n+1} - \bar{q}_h^n}{\Delta t} + \bar{D}_h^\top v_{s_h}^{n+\frac{1}{2}} = 0, \\ (b) \quad \dfrac{h_s}{2T} \dfrac{Q_h^{n+1} - Q_h^n}{\Delta t} + (D_h v_{s_h}^{n+\frac{1}{2}})_{n_q} - j_h^\top v_{p_h}^{n+\frac{1}{2}} = 0, \end{cases} \tag{5.16}$$

where j_h denotes the last column vector of the matrix J_h and n_q is the size of q_h. Since $\bar{M}_h^q$ is diagonal, (5.16a) gives $\bar{q}_h^{n+1}$ explicitly. It remains to solve:

$$\begin{pmatrix} \dfrac{h_s}{T} & -2\Delta t j_h^\top & 0 & 0 \\ \dfrac{\mathcal{R} j_h}{2\Delta t} & I & 0 & \dfrac{\mathcal{R} B_{\omega_h}^\top}{\Delta t} \\ 0 & 0 & M_h^{v_a} & -\Delta t B_{\Gamma_h}^\top \\ 0 & 2B_{\omega_h} & -B_{\Gamma_h} \underline{\mathbf{v}}_{a_h}^{n+1} & 0 \end{pmatrix} \begin{pmatrix} Q_h^{n+1} \\ v_{p_h}^{n+\frac{1}{2}} \\ \underline{\mathbf{v}}_{a_h}^{n+1} \\ \lambda_h^{n+\frac{1}{2}} \end{pmatrix} = \begin{pmatrix} \tilde{Q}_h \\ \tilde{v}_{p_h} \\ \underline{\tilde{\mathbf{v}}}_{a_h} \\ \tilde{\lambda}_h \end{pmatrix}, \tag{5.17}$$

where $\tilde{Q}_h, \tilde{v}_{p_h}, \underline{\tilde{\mathbf{v}}}_{a_h}$ and $\tilde{\lambda}_h$ are known at this step of computations After eliminating $v_{p_h}^{n+\frac{1}{2}}$ and $\underline{\mathbf{v}}_{a_h}^{n+1}$, one obtains:

$$\begin{pmatrix} \dfrac{h_s}{T} + j_h^\top \mathcal{R} j_h & 2 j_h^\top \mathcal{R} B_{\omega_h}^\top \\ \dfrac{B_{\omega_h} \mathcal{R} j_h}{\Delta t} & \dfrac{2}{\Delta t} B_{\omega_h} \mathcal{R} B_{\omega_h}^\top + \Delta t B_{\Gamma_h} (M_h^{v_a})^{-1} B_{\Gamma_h}^\top \end{pmatrix} \begin{pmatrix} Q_h^{n+1} \\ \lambda_h^{n+\frac{1}{2}} \end{pmatrix} = \begin{pmatrix} \tilde{Q}'_h \\ \tilde{\lambda}'_h. \end{pmatrix} \tag{5.18}$$

It remains to eliminate Q_h^{n+1} in this last equation, which leads to:

$$C_\lambda \lambda_h^{n+\frac{1}{2}} = \frac{B_{\omega_h} j_h}{\Delta t (\frac{h_s}{T} + \|j_h\|_{\mathcal{R}}^2)} \tilde{Q}'_h + \tilde{\lambda}'_h. \tag{5.19}$$

where the matrix C_λ is defined by:

$$C_\lambda = \frac{2 B_{\omega_h} \mathcal{R}}{\Delta t} \left(I - \frac{j_h j_h^\top \mathcal{R}}{\frac{h_s}{T} + \|j_h\|_{\mathcal{R}}^2} \right) B_{\omega_h}^\top + \Delta t B_{\Gamma_h} (M_h^{v_a})^{-1} B_{\Gamma_h}^\top \tag{5.20}$$

It will be shown in section (6.1) that C_λ is positive definite under a compatibility condition on the space steps h_a and h_λ. Note that C_λ is small (its dimension is the number of degrees of freedom of λ_h). Once $\lambda_h^{n+\frac{1}{2}}$ is known, $Q_h^{n+1}, v_{p_h}^{n+\frac{1}{2}}, \dot{v}_{p_h}^{n+\frac{1}{2}}$ and $\underline{\mathbf{v}}_{a_h}^{n+1}$ are computed explicitly. Finally, the structure of the global algorithm for the resolution of the scheme (5.14) is the following:

Preliminary computations:

a. Computation of the matrix K_h (Eq.4.7) and of its eigenelements,
b. Computation of the matrix C_λ (Eq. 5.20) and its Cholesky factorization,

At each time step, compute successively:

1. $v_{s_h}^{n+\frac{1}{2}}$, $p_h^{n+\frac{1}{2}}$, $\bar{q}_h^{n+1}$ *with (5.14a), (5.14f) and (5.16a) respectively,*
2. $\lambda_h^{n+\frac{1}{2}}$ *by solving the system (5.19),*
3. Q_h^{n+1} *with the first equation of (5.18),*
4. $v_{p_h}^{n+\frac{1}{2}}$ *with the second equation of (5.17),*
5. $\underline{\mathbf{v}}_{a_h}^{n+1}$ *with the third equation of (5.17),*
6. $\dot{v}_{p_h}^{n+\frac{1}{2}}$ *with (5.14d)*

6. Theoretical issues.

6.1. Existence of the solution. In the algorithm described in the previous section, the existence and uniqueness of the solution is related to the invertibility of the matrix C_λ. In order to show that this matrix is symmetric and positive, it is rewritten in the following form. Since the matrix $\mathcal{R}$ is symmetric and positive (see [17]), one can write $\mathcal{R} = \sqrt{\mathcal{R}}^\top \sqrt{\mathcal{R}}$ so that:

$$C_\lambda = \frac{2B_{\omega_h}\sqrt{\mathcal{R}}^\top}{\Delta t}\left(I - \frac{(\sqrt{\mathcal{R}}^\top j_h)(j_h^\top \sqrt{\mathcal{R}})}{\frac{h_s}{T} + \|j_h\|_{\mathcal{R}}^2}\right)\sqrt{\mathcal{R}}B_{\omega_h}^\top + \Delta t B_{\Gamma_h}(M_h^{v_a})^{-1}B_{\Gamma_h}^\top \tag{6.1}$$

which shows that C_λ is symmetric. In addition, it is easy to verify that:

$$\left(I - \frac{(\sqrt{\mathcal{R}}^\top j_h)(j_h^\top \sqrt{\mathcal{R}})}{\frac{h_s}{T} + \|j_h\|_{\mathcal{R}}^2}\right) = \left(I + \frac{T}{h_s}(\sqrt{\mathcal{R}}^\top j_h)(j_h^\top \sqrt{\mathcal{R}})\right)^{-1} \tag{6.2}$$

and thus C_λ is positive. The fact that it is definite is based on the discrete inf-sup condition of the mixed problem associated to the fictitious domain method. One has to verify:

$$\exists k_0 > 0,\ \inf_{\lambda_h \in \mathcal{L}_h}\sup_{\underline{\mathbf{v}}_{a_h} \in \mathcal{W}_h} \frac{\langle \underline{\mathbf{v}}_a \cdot \underline{\mathbf{N}}, \lambda^* \rangle_\Gamma}{\|\underline{\mathbf{v}}_{a_h}\|_{H(\mathrm{div})}\,\|\lambda\|_{H^{\frac{1}{2}}}} \geq k_0. \tag{6.3}$$

If (6.3) is verified, then B_{Γ_h} is injective so that $B_{\Gamma_h}(M_h^{v_a})^{-1}B_{\Gamma_h}^\top$ is positive definite and consequently C_λ is also positive definite. Notice that the matrix B_{ω_h} is not injective because any line associated to a degree of freedom of λ_h which is not on the soundboard is zero. The condition (6.3) imposes some compatibility between the mesh $\mathcal{C}_h$ of the acoustic domain and the mesh Γ_h of the surface of the guitar. More precisely, it is shown in [31, 25] that assuming that the mesh Γ_h is uniformly regular, then there exists a constant $\alpha > 0$ such that the uniform inf-sup condition (6.3) holds if:

$$h_\lambda \geq \alpha h_a. \tag{6.4}$$

This result does not give any numerical value for the constant α but it depends a priori on the domains $\mathcal{C}$ and Γ. However, in practice, it is verified that the discrete inf-sup condition holds with $\alpha \approx 1.1$.

6.2. Stability analysis.

6.2.1. Discrete energy identity. The stability of the numerical scheme (5.14) is ensured through a fully-discrete energy identity. One has:

THEOREM 6.1 (Energy identity for the numerical scheme). *The solution of (5.14) satisfies:*

$$\frac{E_h^{n+\frac{1}{2}} - E_h^{n-\frac{1}{2}}}{\Delta t} = (\frac{f_{s_h}^{n+1} - f_{s_h}^{n-1}}{2\Delta t}, \overset{\blacktriangle}{v}{}_{s_h}^{n}) - \frac{1}{\Delta t}\int_{t^{n-\frac{1}{2}}}^{t^{n+\frac{1}{2}}} \|\dot{v}_{p_h}\|_{A_h}^2 \tag{6.5}$$

where the total energy $E_h^{n+\frac{1}{2}}$ is defined by $E_h^{n+\frac{1}{2}} = E_{c_h}^{n+\frac{1}{2}} + E_{p_h}^{n+\frac{1}{2}} + E_{a_h}^{n+\frac{1}{2}}$, with:

$$\left|\begin{array}{ll} (a) & E_{c_h}^{n+\frac{1}{2}} = \frac{1}{2}(\overset{\blacktriangle}{v}{}_{s_h}^{n+1}, \overset{\blacktriangle}{v}{}_{s_h}^{n})_{M_h^{v_s}} + \frac{1}{2}\|\overset{\blacktriangle}{q}{}_h^{n+\frac{1}{2}}\|_{M_h^q}^2, \\ (b) & E_{p_h}^{n+\frac{1}{2}} = \frac{1}{2}\|\dot{v}_{p_h}^{n+\frac{1}{2}}\|^2 + \frac{1}{2}\|v_{p_h}^{n+\frac{1}{2}}\|_{A_h}^2, \\ (c) & E_{a_h}^{n+\frac{1}{2}} = \frac{1}{2}\|\underline{\overset{\blacktriangle}{\mathbf{v}}}_{a_h}^{n+\frac{1}{2}}\|_{M_h^{v_a}}^2 + \frac{1}{2}(\overset{\blacktriangle}{p}{}_h^{n+1}, \overset{\blacktriangle}{p}{}_h^{n})_{M_h^p}. \end{array}\right. \tag{6.6}$$

and with the following notations:

$$\begin{array}{ll} \overset{\blacktriangle}{v}{}_{s_h}^{n} = \frac{v_{s_h}^{n+\frac{1}{2}} - v_{s_h}^{n-\frac{1}{2}}}{\Delta t}, & \overset{\blacktriangle}{q}{}_h^{n+\frac{1}{2}} = \frac{q_h^{n+1} - q_h^{n}}{\Delta t} \\ \overset{\blacktriangle}{p}{}_h^{n} = \frac{p_h^{n+\frac{1}{2}} - p_h^{n-\frac{1}{2}}}{\Delta t}, & \underline{\overset{\blacktriangle}{\mathbf{v}}}_{a_h}^{n+\frac{1}{2}} = \frac{\underline{\mathbf{v}}_{a_h}^{n+1} - \underline{\mathbf{v}}_{a_h}^{n}}{\Delta t} \end{array} \tag{6.7}$$

Proof. First, (5.13) is multiplied by $\dot{v}_{p_h}$, integrated in time on $[t^{n-\frac{1}{2}}, t^{n+\frac{1}{2}}]$ and the result is divided by Δt. Since $\frac{\lambda_h^{n+\frac{1}{2}} - \lambda_h^{n-\frac{1}{2}}}{\Delta t}$ and $\frac{q_h^{n+1} - q_h^{n-1}}{2\Delta t}$ are constant on the integration interval, this leads to:

$$\begin{aligned} \frac{E_{p_h}^{n+\frac{1}{2}} - E_{p_h}^{n-\frac{1}{2}}}{\Delta t} = -\frac{1}{\Delta t}\int_{t^{n-\frac{1}{2}}}^{t^{n+\frac{1}{2}}} \|\dot{v}_{p_h}\|_{A_h}^2 - (J_h\frac{q_h^{n+1} - q_h^{n-1}}{2\Delta t}, \frac{v_{p_h}^{n+\frac{1}{2}} - v_{p_h}^{n-\frac{1}{2}}}{\Delta t}) \\ - (B_{\omega_h}^\top \frac{\lambda_h^{n+\frac{1}{2}} - \lambda_h^{n-\frac{1}{2}}}{\Delta t}, \frac{v_{p_h}^{n+\frac{1}{2}} - v_{p_h}^{n-\frac{1}{2}}}{\Delta t}), \end{aligned} \tag{6.8}$$

Then (5.14a), (5.14b), (5.14e) and (5.14f) are differentiated in discrete time:

$$\left\{\begin{array}{ll} (a) & M_h^{v_s}\frac{\overset{\blacktriangle}{v}{}_{s_h}^{n+1} - \overset{\blacktriangle}{v}{}_{s_h}^{n}}{\Delta t} - D_h\overset{\blacktriangle}{q}{}_h^{n+\frac{1}{2}} = \frac{f_{s_h}^{n+1} - f_{s_h}^{n}}{\Delta t}, \\ (b) & M_h^q\frac{\overset{\blacktriangle}{q}{}_h^{n+\frac{1}{2}} - \overset{\blacktriangle}{q}{}_h^{n-\frac{1}{2}}}{\Delta t} + D_h^\top\overset{\blacktriangle}{v}{}_{s_h}^{n} - J_h^\top\frac{v_{p_h}^{n+\frac{1}{2}} - v_{p_h}^{n-\frac{1}{2}}}{\Delta t} = 0, \\ (c) & M_h^{v_a}\frac{\underline{\overset{\blacktriangle}{\mathbf{v}}}_{a_h}^{n+\frac{1}{2}} - \underline{\overset{\blacktriangle}{\mathbf{v}}}_{a_h}^{n-\frac{1}{2}}}{\Delta t} - G_h\overset{\blacktriangle}{p}{}_h^{n} - (B_{\Gamma_h})^\top\frac{\lambda_h^{n+\frac{1}{2}} - \lambda_h^{n-\frac{1}{2}}}{\Delta t} = 0, \\ (d) & M_h^p\frac{\overset{\blacktriangle}{p}{}_h^{n+1} - \overset{\blacktriangle}{p}{}_h^{n}}{\Delta t} + G_h^\top\underline{\overset{\blacktriangle}{\mathbf{v}}}_{a_h}^{n+\frac{1}{2}} = 0, \end{array}\right. \tag{6.9}$$

Equation (6.9b) is multiplied by $\frac{\overset{\blacktriangle}{q}_h^{n+\frac{1}{2}} + \overset{\blacktriangle}{q}_h^{n-\frac{1}{2}}}{2} = \frac{q_h^{n+1} - q_h^{n-1}}{2\Delta t}$, which leads to:

$$\frac{\frac{1}{2}\|\overset{\blacktriangle}{q}_h^{n+\frac{1}{2}}\|^2_{M_h^q} - \frac{1}{2}\|\overset{\blacktriangle}{q}_h^{n-\frac{1}{2}}\|^2_{M_h^q}}{\Delta t} + (D_h^\top \overset{\blacktriangle}{v}_{s_h}^n, \frac{\overset{\blacktriangle}{q}_h^{n+\frac{1}{2}} + \overset{\blacktriangle}{q}_h^{n-\frac{1}{2}}}{2}) - (J_h^\top \frac{v_{p_h}^{n+\frac{1}{2}} - v_{p_h}^{n-\frac{1}{2}}}{\Delta t}, \frac{q_h^{n+1} - q_h^{n-1}}{2\Delta t}) = 0. \tag{6.10}$$

The equation (6.9c) is multiplied by $\frac{\overset{\blacktriangle}{\underline{\mathbf{v}}}_{a_h}^{n+\frac{1}{2}} + \overset{\blacktriangle}{\underline{\mathbf{v}}}_{a_h}^{n-\frac{1}{2}}}{2} = \frac{\underline{\mathbf{v}}_{a_h}^{n+1} - \underline{\mathbf{v}}_{a_h}^{n-1}}{2\Delta t}$:

$$\frac{\frac{1}{2}\|\overset{\blacktriangle}{\underline{\mathbf{v}}}_{a_h}^{n+\frac{1}{2}}\|^2_{M_h^{v_a}} - \frac{1}{2}\|\overset{\blacktriangle}{\underline{\mathbf{v}}}_{a_h}^{n+\frac{1}{2}}\|^2_{M_h^{v_a}}}{\Delta t} - (G_h \overset{\blacktriangle}{p}_h^n, \frac{\overset{\blacktriangle}{\underline{\mathbf{v}}}_{a_h}^{n+\frac{1}{2}} + \overset{\blacktriangle}{\underline{\mathbf{v}}}_{a_h}^{n-\frac{1}{2}}}{2}) - (B_{\Gamma_h}^\top \frac{\lambda_h^{n+\frac{1}{2}} - \lambda_h^{n-\frac{1}{2}}}{\Delta t}, \frac{\underline{\mathbf{v}}_{a_h}^{n+1} - \underline{\mathbf{v}}_{a_h}^{n-1}}{2\Delta t}) = 0. \tag{6.11}$$

The mean value of (6.9a) written at times $t^{n-\frac{1}{2}}$ and $t^{n+\frac{1}{2}}$ is multiplied by $\overset{\blacktriangle}{v}_{s_h}^n$:

$$\frac{\frac{1}{2}(\overset{\blacktriangle}{v}_{s_h}^{n+1}, \overset{\blacktriangle}{v}_{s_h}^n)_{M_h^{v_s}} - \frac{1}{2}(\overset{\blacktriangle}{v}_{s_h}^n, \overset{\blacktriangle}{v}_{s_h}^{n-1})_{M_h^{v_s}}}{\Delta t} - (D_h \frac{\overset{\blacktriangle}{q}_h^{n+\frac{1}{2}} + \overset{\blacktriangle}{q}_h^{n-\frac{1}{2}}}{2}, \overset{\blacktriangle}{v}_{s_h}^n) = (\frac{f_{s_h}^{n+1} - f_{s_h}^{n-1}}{2\Delta t}, \overset{\blacktriangle}{v}_{s_h}^n) \tag{6.12}$$

and the mean value of (6.9d) written at times $t^{n-\frac{1}{2}}$ and $t^{n+\frac{1}{2}}$ is multiplied by $\overset{\blacktriangle}{p}_h^n$

$$\frac{\frac{1}{2}(\overset{\blacktriangle}{p}_h^{n+1}, \overset{\blacktriangle}{p}_h^n)_{M_h^p} - \frac{1}{2}(\overset{\blacktriangle}{p}_h^n, \overset{\blacktriangle}{p}_h^{n-1})_{M_h^p}}{\Delta t} + (G_h^\top \frac{\overset{\blacktriangle}{\underline{\mathbf{v}}}_{a_h}^{n+\frac{1}{2}} + \overset{\blacktriangle}{\underline{\mathbf{v}}}_{a_h}^{n-\frac{1}{2}}}{2}, \overset{\blacktriangle}{p}_h^n) = 0. \tag{6.13}$$

Finally, the sum of equations (6.8), (6.10), (6.11), (6.12) and (6.13) gives:

$$\frac{E_h^{n+\frac{1}{2}} - E_h^{n-\frac{1}{2}}}{\Delta t} = \left(\frac{f_{s_h}^{n+1} - f_{s_h}^{n-1}}{2\Delta t}, \overset{\blacktriangle}{v}_{s_h}^n\right) - \frac{1}{\Delta t}\int_{t^{n-\frac{1}{2}}}^{t^{n+\frac{1}{2}}} \|\dot{v}_{p_h}\|^2_{A_h} + (\frac{\lambda_h^{n+\frac{1}{2}} - \lambda_h^{n-\frac{1}{2}}}{\Delta t}, B_{\Gamma_h}\frac{\underline{\mathbf{v}}_{a_h}^{n+1} - \underline{\mathbf{v}}_{a_h}^{n-1}}{2\Delta t} - B_{\omega_h}\frac{v_{p_h}^{n+\frac{1}{2}} - v_{p_h}^{n-\frac{1}{2}}}{\Delta t}) \tag{6.14}$$

and the time discretization of (5.10f) has been determined so that the last term of this equation is zero.

□

6.2.2. Stability conditions for the numerical scheme. The identity (6.5) shows that the discrete energy $E_h^{n+\frac{1}{2}}$ is decaying as soon as the force exerted by the finger on the string is zero. It is thus possible to derive conditions which ensure that the discrete energy is positive and consequently the stability of the scheme [4]. One has the following result:

THEOREM 6.2 (Stability of the discrete scheme (5.14)). *Assuming that the discrete inf-sup condition (6.3) is verified, one has:*

- *the discrete energy of the string* $E_{c_h}^{n+\frac{1}{2}}$*, defined in (6.6a) is positive if:*

$$\frac{c_s \Delta t}{h_s} < 1, \tag{6.15}$$

- *the discrete energy of the plate* $E_{p_h}^{n+\frac{1}{2}}$*, defined in (6.6b) is always positive;*
- *the discrete energy of the air* $E_{a_h}^{n+\frac{1}{2}}$*, defined in (6.6c) is positive if:*

$$\frac{c_a \Delta t}{h_a} < \frac{1}{\sqrt{3}}. \tag{6.16}$$

When both conditions (6.15) and (6.16) are satisfied, the scheme (5.14) is stable.
Proof.
1. One has:

$$\left(\overset{\blacktriangle}{v}_{s_h}^{n+1}, \overset{\blacktriangle}{v}_{s_h}^{n} \right)_{M_h^{v_s}} = \frac{1}{4} \left[\| \overset{\blacktriangle}{v}_{s_h}^{n+1} + \overset{\blacktriangle}{v}_{s_h}^{n} \|_{M_h^{v_s}}^2 - \| \overset{\blacktriangle}{v}_{s_h}^{n+1} - \overset{\blacktriangle}{v}_{s_h}^{n} \|_{M_h^{v_s}}^2 \right], \tag{6.17}$$

thus, using (5.14a) one obtains:

$$2E_{c_h}^{n+\frac{1}{2}} \geq \left(1 - \frac{\alpha_h \Delta t^2}{4} \right) \| q_h \|_{M_h^q}^2 + \| \frac{\overset{\blacktriangle}{v}_{s_h}^{n+1} + \overset{\blacktriangle}{v}_{s_h}^{n}}{2} \|_{M_h^{v_s}}^2 \tag{6.18}$$

where:

$$\alpha_h = \sup_{q_h \in \mathcal{Q}_h} \frac{\left(D_h q_h, (M_h^{v_s})^{-1} D_h q_h \right)}{\| q_h \|_{M_h^q}^2}. \tag{6.19}$$

The energy of the string is then positive as soon as:

$$\frac{\alpha_h \Delta t^2}{4} < 1. \tag{6.20}$$

Using the uniformity of the string mesh, a standard Fourier analysis technique leads to the usual estimation [14]:

$$\alpha_h \leq \frac{4c_s^2}{h_s^2} + O(1),$$

from which the condition (6.15) is deduced.

2. Using the same technique, one shows, with the help (5.14f), that:

$$2E_{a_h}^{n+\frac{1}{2}} \geq \left(1 - \frac{\alpha_h \Delta t^2}{4} \right) \| \underline{\mathbf{v}}_{a_h} \|_{M_h^{v_a}}^2 + \| \frac{\overset{\blacktriangle}{p}_h^{n+1} + \overset{\blacktriangle}{p}_h^{n}}{2} \|_{M_h^p}^2 \tag{6.21}$$

where:

$$\alpha_h = \sup_{\underline{\mathbf{v}}_{a_h} \in \mathcal{W}_h} \frac{\left(G_h^\top \underline{\mathbf{v}}_{a_h}, (M_h^p)^{-1} G_h^\top \underline{\mathbf{v}}_{a_h} \right)}{\| \underline{\mathbf{v}}_{a_h} \|_{M_h^{v_a}}^2}. \tag{6.22}$$

Using the uniformity of the mesh of the acoustic domain, a standard Fourier analysis technique leads to the usual estimation:

$$\alpha_h \leq \frac{12c_a^2}{h_a^2} + O(1),$$

from which the condition (6.16) is deduced. □

7. Numerical simulations.

7.1. Choice of the discretization parameters. For the numerical experiments, the values of the various physical and geometrical parameters used correspond to standard values found in the existing literature (in particular in [38] for the wood parameters of the soundboard). They are given in table Table. 7.1.

TABLE 7.1
Values of geometrical and physical parameters used for the simulations

String: $\rho_s = 0.00525\ kg.m^{-1}, \quad T = 60N, \quad l_s = 65cm,\ \eta_s = 9.10^{-8}s.$

Soundboard:

	c_{11} (MPa)	$c_{11}\tilde{c}_{22}$ (MPa)	$c_{11}\tilde{c}_{12}$ (MPa)	$c_{11}\tilde{c}_{33}$ (MPa)	ρ_p $(kg.m^{-1})$	a (mm)	η_p (s)
plate	850	50	75	200	350	2.9	0.005
bridge	80	50	900	270	400	6	0.005
struts	100	60	1250	300	400	14	0.005

Air: $c_a = 344m.s^{-1}, \quad \rho_a = 1.21kgm^{-3},$

Force at the bridge: $G(x,y) = \delta_{(x_0,y_0)} \quad (x_0,y_0) = (65cm, 4cm).$

Plucking force: $f_s(x,t) = g(x)h(t).$

$$g(x) = \frac{\exp(-(x - x_f/\delta_f)^2)}{\int_0^{l_s} \exp(-(x - x_f/\delta_f)^2)} \qquad h(t) = \begin{cases} (1 - \cos(\pi t/t_1)), & 0 \le t \le t_1, \\ (1 + \cos(\pi(t - t_1)/t_2)), & t_1 \le t \le t_2, \\ 0, & t > t_2. \end{cases}$$

$x_f = 55cm, \quad \delta_f = 6mm, \quad t_1 = 15ms \quad t_2 = 0.4ms.$

The discretization parameters are chosen in order to verify the different constraints given by the stability conditions and the inf-sup criterion.

1. A mesh of the soundboard ω_h including 3 struts and a bridge is constructed with space step $h_p = 1.2cm$ (Fig. 7.1a). The number of vertices of this mesh is 571 and the number of degrees of freedom is 3230. The number of modes of the soundboard plate operator used is 50, which correspond to a cut frequency of nearly 3000 Hz.
2. In order to simplify the computation of the coupling matrix B_{ω_h}, the mesh Γ_h of the surface of the guitar is an extension of the soundboard's mesh (Fig. 7.1b).. Since the rigid part of the body does not present small parts, one has: $h_\lambda = h_p$. The number of degrees of freedom of this mesh is 1260.
3. The space step in the air h_a is then chosen according the heuristic criterion $h_\lambda > 1.1h_a$, imposed by the uniform inf-sup discrete condition (6.3): $h_a = 1.1cm$. The computational domain is a box with side length 90 cms. This lead to a mesh containing approximately 440,000 cubes.
4. The time step must verify the CFL condition (6.16), which lead to $\Delta t = 1.85\,10^{-5}s$. The sampling frequency is thus $50962Hz$, which lead for a 6s duration computation to nearly 300,000 time steps.
5. Finally, the space step in the string is chosen in adequation with the CFL condition (6.15). For the lowest E6 string (fundamental 82.6 Hz), one has thus $h_s = 2.1mm$ which corresponds to 308 nodes.

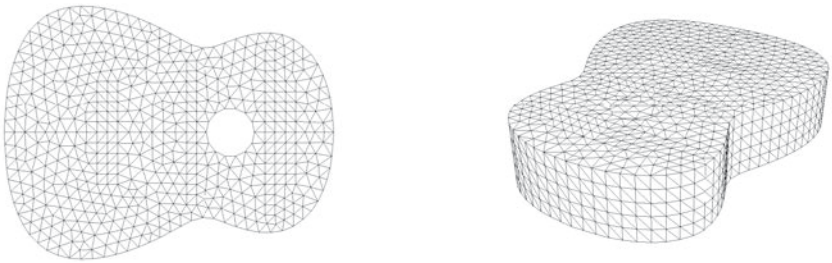

(a) (b)

FIG. 7.1. *(a) Mesh of the soundboard ω with 3 cross struts and the bridge (b) Mesh of the surface of the guitar Γ*

7.2. Results. We present here a couple of numerical results: eigenmodes of the soundboard *in vacuo*, energy curves and visualization of the unknowns just after the plucking. We refer the reader to a previous paper [18] in which a frequency analysis of the simulation results is performed in order to evaluate the transfer of energy through the various components of the coupled system and the effect of some structural changes is presented which allows to analyze the vibroacoustical behavior of the guitar in terms of structural, acoustic and structural-acoustic modes.

7.2.1. First eigenmodes of the soundboard in vacuo . The measurement of the eigenfrequencies and eigenmodes of the soundboard of a guitar has been the subject of an important number of experiments [30, 41, 35]. In the present study, the purpose was not to simulate a particular instrument. Nevertheless it is possible to compare at least qualitatively the shape and frequencies of the simulated soundboard to existing results. Figure 7.2 shows the first 5 modes of a classical guitar soundboard clamped on its outer boundary and without cavity, observed by Jansson and Fig. 7.3 shows the first six modes computed using the second order space approximation. One can see that the computed modes are in good agreement with the experiments, both for the shape and the frequencies estimations. The addition of an extra mode comparing to the real guitar is certainly due to a rather simple strutting modeling of the simulated soundboard.

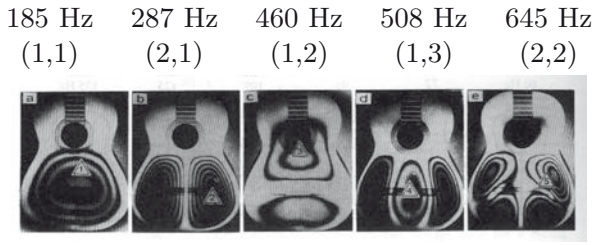

FIG. 7.2. *Vibration modes of a classical guitar top plate glued to fixed ribs and without back (Jansson, 1971 [30])*

7.2.2. Energy. Figure Fig. 7.4 shows the evolution of the energy during 100 ms when plucking the lowest string of the guitar. The energy of the complete system and the energy of the substructures of the instrument (string, plate and air) are represented. Since the string remains the essential part of the total energy, the plate

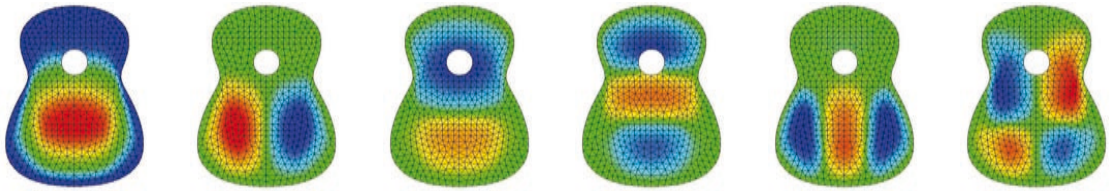

181 Hz *289 Hz* *309 Hz* *448 Hz* *532 Hz* *586 Hz*
(1,1) *(2,1)* *(1,2)* *(1,3)* *(3,1)* *(2,2)*

FIG. 7.3. *Computed vibration modes of the soundboard* in vacuo

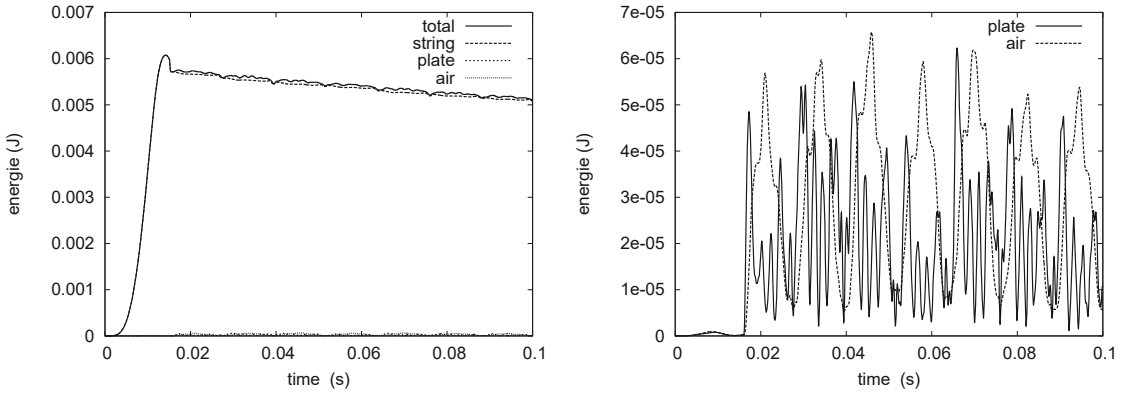

(a) (b)

FIG. 7.4. *(a) Evolution of the energy of string, plate, air and total energy vs time for the plucked open string E_2 (fundamental 82.6 Hz) during the first 100ms of the tone.(b) Plate and air energy represented with appropriate scale.*

and air energy are scaled by a factor 70. During the plucking, the string receives mechanical energy from the finger. One can see that only a small part of this energy in then transmitted to the plate and to the air. These curves show the energy exchange between string plate and air.

27

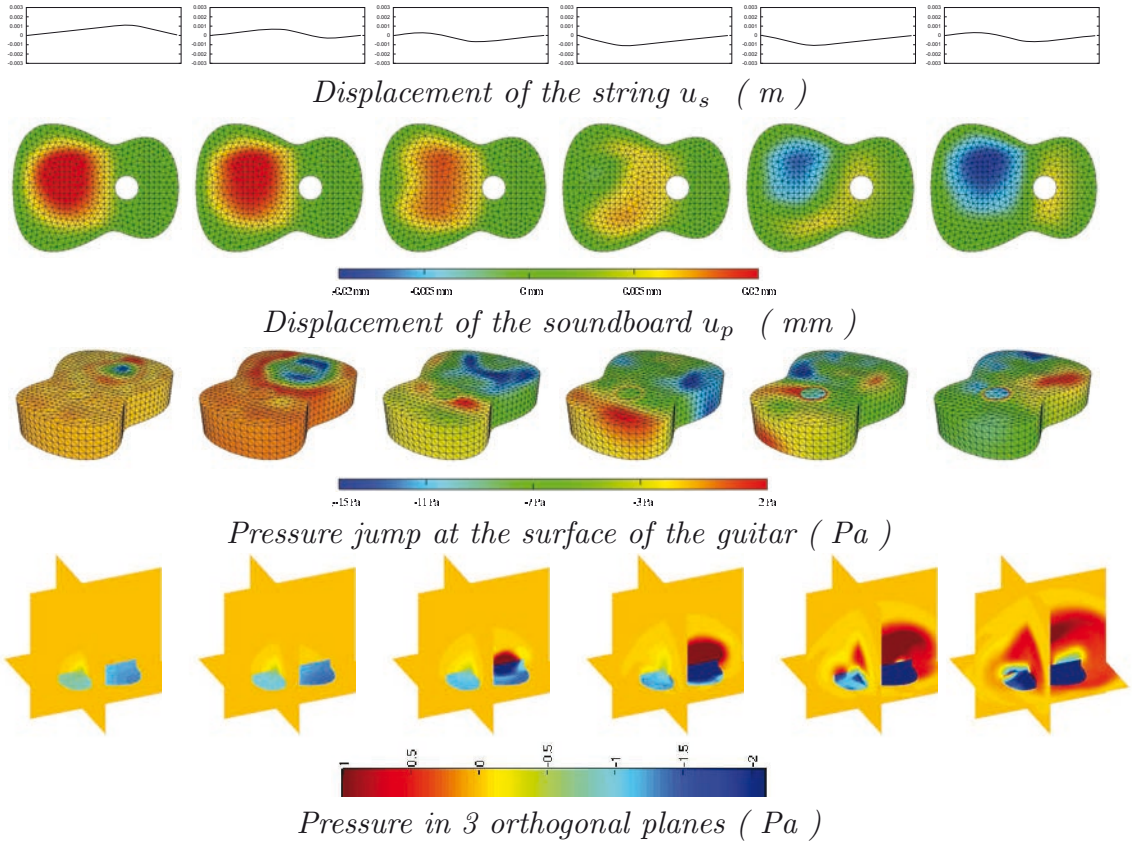

FIG. 7.5. *String displacement, plate displacement, pressure jump and pressure in 3 orthogonal planes immediately after the plucking of the open lowest string (E6, fundamental 82.5 Hz).*

7.2.3. Visualization of the unknowns. Figure 7.5 shows the evolution of the solution immediately after the plucking of the string, that is at the very beginning of the free vibrations. The following quantities are represented:

- the string displacement,
- the plate displacement,
- the pressure jump λ_h at the surface of the guitar,
- the pressure p in 3 orthogonal planes simultaneously, which intersect in the middle of the cavity, under the hole.

The time duration between two pictures is 0.36ms. The time evolution of the quantities is obviously better seen with animated pictures [6]. The pictures of plate displacement and of the pressure jump have been realized with the software Medit [24]. Note that the pressure in the cavity is largely greater than the pressure outside. The pressure across the surface presents thus important variations near the hole, since the pressure is obviously continuous across the hole. The amplitude of the string is approximately 2mm and the amplitude of the soundboard is only of the order of 20 μm.

8. Conclusion. We have presented a relatively exhaustive numerical modeling of the acoustic guitar. Up to our knowledge, this is the first modeling of this instrument which involves the whole vibroacoustical behavior from the initial pluck to the 3D acoustic radiation. Among other things, this numerical method can be used as a tool for the estimation of quantities that are hard to measure experimentally as for example the estimation of the relative structural losses and radiation losses in the sounds generated by the guitar [18]. It can also be seen from Fig. 7.5 that the

simulation results can be used for the analysis of the directivity properties of the instrument.

This work has been made possible with the help of recent research developed in numerical methods. It must be pointed out that the complex geometry of the instrument for the fluid-structure interaction part of the problem is taken into account in a very efficient way via the fictitious domain method. Also, the problem is limited to a bounded cube with the help of high order absorbing boundary conditions. The most interesting aspect of this study is certainly the stability analysis which is based on energy estimation derived from the numerical scheme. This efficient technique permits to show the stability in the rather complicated case where different time-discretization are used, namely an analytical one and a finite differences one. Furthermore, for the particular scheme presented here, the stability conditions are optimal in the sense that they are the same than the ones obtained for uncoupled schemes.

REFERENCES

[1] J. Argyris, I. Fried, and D. Sharpf, *The TUBA family of plate elements for thematrix displacement method*, The Aeronaultical Journal of the Royal Aeronautical Society, 72 (1968), pp. 701–709.

[2] G. P. Astrakhantsev, *Method of fictitious domain method for a second-order elliptic equation with natural boundary conditions*, USRR Compu. Math. and Math. Phys., 18 (1978), pp. 114–121.

[3] I. Babuska, *The Finite Element Method with Lagrangian Multipliers*, Numer. Math., 20 (1973), pp. 179–192.

[4] A. Bamberger, G. Chavent, and P. Lailly, *Etude de schémas numériques pour les équations de l' élastodynamique linéaire*, Tech. Report 41, INRIA, 1980. Rapport Interne.

[5] J. Batoz, K. Bathe, and L. . Ho, *A study of three-node triangular plate bending elements*, International Journal for Numerical Methods in Enginerering, 15(2) (1980).

[6] E. Bécache, A. Chaigne, G. Derveaux, and P. Joly, *Numerical simulation of the acoustic guitar*. DVD, VHS and RealPlayer document, English, March 2003. http://www.inria.fr/multimedia/Videotheque-fra.html.

[7] E. Bécache, P. Joly, and C. Tsogka, *Fictitious domains, mixed finite elements and perfectly matched layers for 2d elastic wave propagation*, J. Comp. Acous., 9 (2001), pp. 1175–1203.

[8] F. Brezzi and M. Fortin, *Numerical approximation of mindlin-reissner plates*, Mathematics of computation, 47(175) (1986), pp. 151–158.

[9] A. Chaigne, *On the use of finite differences for musical synthesis. Application to plucked string instruments* , J. Acoust., 5 (1992), pp. 181–211.

[10] A. Chaigne and C. Lambourg, *Time-domain simulation of damped impacted plates. Part I. Theory and experiments*, J. Acoust. Soc. Am., 109 (2001), pp. 1422–1432.

[11] D. Chapelle, *Une formulation mixte de plaque ou l'effort tranchant est approché dans son espace naturel*, tech. report, INRIA, 1993.

[12] P. Ciarlet, *The finite element method for elliptic problems*, North Holland, eds, 1978.

[13] P. G. Ciarlet, *Mathematical elasticity. Vol. II*, North-Holland Publishing Co., Amsterdam, 1997. Theory of plates.

[14] G. Cohen, *Higher-Order Numerical Methods for Transient Wave Equations*, Springer, 2002.

[15] G. Cohen, P. Joly, J. E. Roberts, and N. Tordjman, *Higher order triangular finite elements with mass lumping for the wave equation*, SIAM J. Numer. Anal., 38 (2001), pp. 2047–2078 (electronic).

[16] F. Collino, *Conditions absorbantes d'ordre élevé pour des modèles de propagation d'onde dans des domaines rectangulaires*, Tech. Report 1790, INRIA, Novembre 1992.

[17] G. Derveaux, *Modélisation numérique de la guitare acoustique* , PhD thesis, Ecole Polytechnique, 2002.

[18] G. Derveaux, A. Chaigne, P. Joly, and E. Bécache, *Time-domain simulation of a guitar : model and method* , J. Acoust. Soc. Am., 114 (2003), pp. 3368 – 3383.

[19] P. Destuynder and T. Nevers, *A new finite element for bending plates*, Computer Methods in Applied Mechanics and Engineering, 68 (1988).

[20] P. Destuynder and M. Salaun, *Mathematical analysis of thin plate models*, vol. 24 of Mathématiques & Applications (Berlin) [Mathematics & Applications], Springer-Verlag,

Berlin, 1996.
[21] B. Engquist and A. Majda, *Absorbing boundary conditions for the numerical simulation of waves*, Math. Comp., 31 (1977), pp. 629–651.
[22] P. C. et P.A. Raviart, *A mixed finite element method for the biharmonic equation*, in Mathematical Aspects of Finite Elements in Partial Differential Equations, C. de Boor, ed., Academic Press, 1974, pp. 125–145.
[23] N. H. Fletcher and T. D. Rossing, *The physics of musical instruments*, Springer-Verlag, New York, second ed., 1998.
[24] P. J. Frey, *Medit: An interactive mesh visualization software.* www.http://www-rocq1.inria.fr/gamma/medit/.
[25] V. Girault and R. Glowinski, *Error analysis of a fictitious domain method applied to a Dirichlet problem*, Japan J. Indust. Appl. Math., 12 (1995), pp. 487–514.
[26] R. Glowinski, *Approximations externes,par éléments finis de lagrange d'ordre un et deux, du problème de dirichlet pour l'opérateur biharmonique. méthodes itératives de résolution des problèmes approchés.*, in Topics in Numerical Analysis, J. Miller, ed., Academic Press, 1973, pp. 123–171.
[27] R. Glowinski, T. Pan, and J. Periaux, *A fictitious domain method for external incompressible viscous flow modeled by Navier-Stokes equations*, Comp. Meth. in Appl. Mech. and Eng., 112 (1994), pp. 133–148.
[28] R. Glowinski, T. Pan, and J. Periaux, *A fictitious domain method for dirichlet problem and applications*, Comp. Meth. in Appl. Mech. and Engin., 111 (1994), pp. 283–304.
[29] T. Hughes, *The finite element method: Linear static and dynamic finite element analysis*, Prentice-Hall, 1987.
[30] E. Jannson, *A study of acoustical and hologram interferometric measurements on the top plate vibrations of of a guitar* , Acustica, 25 (1971).
[31] P. Joly and L. Rhaouti, *Domaines fictifs, éléments finis* H(div) *et condition de Neumann: le problème de la condition inf-sup*, C. R. Acad. Sci. Paris Sér. I Math., 328 (1999), pp. 1225–1230.
[32] Y. A. Kuznetsov, *Fictitious component and domain decomposition methods for the solution of eigenvalue problems*, in Computing methods in applied sciences and engineering, VII (Versailles, 1985), North-Holland, Amsterdam, 1986, pp. 155–172.
[33] A. W. Leissa, *Vibrations of plates*, NASA SP, 160 (1969).
[34] F. Millot, F. Collino, and P. Joly, *Fictitious domain method for unsteady problems: application to electromagnetic scattering*, in Mathematical and numerical aspects of wave propagation (Mandelieu-La Napoule, 1995), SIAM, Philadelphia, PA, 1995, pp. 260–269.
[35] C. S. M.J. Elejabarrieta, A. Ezcurra, *Evolution of the vibrational behavior of a guitar sounboard along successive construction phases by means of the modal analysis technique* , J. Acoust. Soc. Am., 108 (2000), pp. 369–378.
[36] J. Pitkäranta, *Boundary Subspaces for the Finite Element Method With Lagrange Multipliers*, Numer. Math., 33 (1979), pp. 273–289.
[37] L. Rhaouti, A. Chaigne, and P. Joly, *Time-domain simulation and numerical modeling of the kettledrum* , J. Acoust. Soc. Am., 105 (1999), pp. 3545 – 3562.
[38] B. Richardson and G. Roberts, *The adjustment of mode frequencies in guitars: A study by means of holographic interferometry and finite element analysis*, in SMAC 83, vol. 2, Stockholm, Sweden, July 1983, pp. 285–302.
[39] B. E. Richardson, *The influence of strutting of the top-plate of a guitar*, Catgut Acoustical Soc. Newsletter, 40 (1983), pp. 13–17.
[40] B. E. Richardson, *The acoustical development of the guitar* , Catgut Acoust. Soc. J., 2 (1994), pp. 181–211.
[41] T. D. Rossing and G. Eban, *Normal modes of a radially braced guitar determined by TV holography*, J. Acoust. Soc. Am., 106 (1999), pp. 2991–2996.
[42] K. Yosida, *Functional Analysis*, Springer, 1965.